THE JOURNAL OF PHYSICAL CHEMISTRY A

Article

pubs.acs.org/JPCA

1,2-Dichlorohexafluoro-cyclobutane (1,2-c-$C_4F_6Cl_2$, R-316c) a Potent Ozone Depleting Substance and Greenhouse Gas: Atmospheric Loss Processes, Lifetimes, and Ozone Depletion and Global Warming Potentials for the (*E*) and (*Z*) Stereoisomers

Vassileios C. Papadimitriou,[†,‡,§] Max R. McGillen,[†,‡] Shona C. Smith,[†,‡] Aaron M. Jubb,[†,‡] Robert W. Portmann,[†] Bradley D. Hall,[∥] Eric L. Fleming,[⊥,#] Charles H. Jackman,[⊥] and James B. Burkholder*[,†]

[†]Earth System Research Laboratory, Chemical Sciences Division, National Oceanic and Atmospheric Administration, 325 Broadway, Boulder, Colorado, 80305 United States

[‡]Cooperative Institute for Research in Environmental Sciences, University of Colorado, Boulder, Colorado, 80309 United States

[§]Laboratory of Photochemistry and Chemical Kinetics, Department of Chemistry, University of Crete, Vassilika Vouton, 71003 Heraklion, Crete, Greece

[∥]Earth System Research Laboratory, Global Monitoring Division, National Oceanic and Atmospheric Administration, 325 Broadway, Boulder, Colorado, 80305 United States

[⊥]NASA Goddard Space Flight Center, Greenbelt, Maryland, 20771 United States

[#]Science Systems and Applications, Inc., Lanham, Maryland, 20706 United States

Supporting Information

ABSTRACT: The atmospheric processing of (*E*)- and (*Z*)-1,2-dichlorohexafluoro-cyclobutane (1,2-c-$C_4F_6Cl_2$, R-316c) was examined in this work as the ozone depleting (ODP) and global warming (GWP) potentials of this proposed replacement compound are presently unknown. The predominant atmospheric loss processes and infrared absorption spectra of the R-316c isomers were measured to provide a basis to evaluate their atmospheric lifetimes and, thus, ODPs and GWPs. UV absorption spectra were measured between 184.95 to 230 nm at temperatures between 214 and 296 K and a parametrization for use in atmospheric modeling is presented. The Cl atom quantum yield in the 193 nm photolysis of R-316c was measured to be 1.90 ± 0.27. Hexafluorocyclobutene (c-C_4F_6) was determined to be a photolysis co-product with molar yields of 0.7 and 1.0 (±10%) for (*E*)- and (*Z*)-R-316c, respectively. The 296 K total rate coefficient for the $O(^1D)$ + R-316c reaction, i.e., $O(^1D)$ loss, was measured to be $(1.56 \pm 0.11) \times 10^{-10}$ cm^3 molecule^{-1} s^{-1} and the reactive rate coefficient, i.e., R-316c loss, was measured to be $(1.36 \pm 0.20) \times 10^{-10}$ cm^3 molecule^{-1} s^{-1} corresponding to a ~88% reactive yield. Rate coefficient upper-limits for the OH and O_3 reaction with R-316c were determined to be $<2.3 \times 10^{-17}$ and $<2.0 \times 10^{-22}$ cm^3 molecule^{-1} s^{-1}, respectively, at 296 K. The quoted uncertainty limits are 2σ and include estimated systematic errors. Local and global annually averaged lifetimes for the (*E*)- and (*Z*)-R-316c isomers were calculated using a 2-D atmospheric model to be 74.6 ± 3 and 114.1 ± 10 years, respectively, where the estimated uncertainties are due solely to the uncertainty in the UV absorption spectra. Stratospheric photolysis is the predominant atmospheric loss process for both isomers with the $O(^1D)$ reaction making a minor, ~2% for the (*E*) isomer and 7% for the (*Z*) isomer, contribution to the total atmospheric loss. Ozone depletion potentials for (*E*)- and (*Z*)-R-316c were calculated using the 2-D model to be 0.46 and 0.54, respectively. Infrared absorption spectra for (*E*)- and (*Z*)-R-316c were measured at 296 K and used to estimate their radiative efficiencies (REs) and GWPs; 100-year time-horizon GWPs of 4160 and 5400 were obtained for (*E*)- and (*Z*)-R-316c, respectively. Both isomers of R-316c are shown in this work to be long-lived ozone depleting substances and potent greenhouse gases.

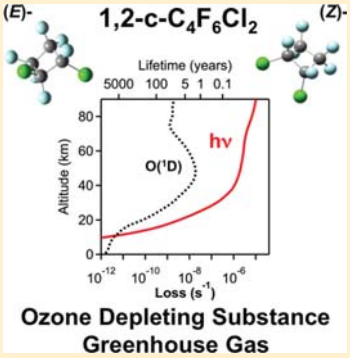

1. INTRODUCTION

The Montreal Protocol and its subsequent amendments phased-out production of a number of chlorofluorocarbons (CFCs), e.g., $CFCl_3$ (CFC-11) and CF_2Cl_2 (CFC-12), due to their role in the depletion of stratospheric ozone. The chlorofluorocarbon 1,2-dichlorohexafluoro-cyclobutane, (*E*)- and (*Z*)-1,2-c-$C_4F_6Cl_2$ (R-316c), which is not included under the Montreal Protocol, is currently used in limited quantities as a nonimmobilizer amnestic drug[1,2] in medical research and is currently under consideration for use in commercial applications. The environmental impact of

Received: August 5, 2013
Revised: September 27, 2013
Published: September 30, 2013

   dx.doi.org/10.1021/jp407823k | *J. Phys. Chem. A* 2013, 117, 11049−11065

R-316c and its atmospheric removal processes are, however, presently not well characterized. Prior to commercial use, a thorough environmental impact assessment of the (*E*) and (*Z*) isomers of R-316c that includes, in particular, an evaluation of their atmospheric lifetime as well as ozone depletion (ODP) and global warming (GWP) potentials is therefore warranted. In this study, the primary atmospheric loss processes of 1,2-c-$C_4F_6Cl_2$ have been quantified to provide a basis for an evaluation.

Chlorofluorocarbons (CFCs) are primarily removed in the stratosphere by UV photolysis at wavelengths less than 230 nm

$$1,2\text{-c-}C_4F_6Cl_2 + h\nu \rightarrow \text{products} \quad (1)$$

with photolysis rates being greater for molecules with a greater degree of chlorination. Molecules that are primarily removed in the stratosphere are relatively long-lived with atmospheric lifetimes greater than ∼40 years or so. CFCs are also removed in the stratosphere by reaction with $O(^1D)$

$$O(^1D) + 1,2\text{-c-}C_4F_6Cl_2 \rightarrow O(^3P) + 1,2\text{-c-}C_4F_6Cl_2(\text{quenching}) \quad (2a)$$

$$\rightarrow O(^3P) + \text{products(reactive quenching)} \quad (2b)$$

$$\rightarrow \text{products(reaction)} \quad (2c)$$

where channels 2b and 2c lead to the atmospheric loss of 1,2-c-$C_4F_6Cl_2$. Other gas-phase reactive loss processes for CFCs are expected to be negligible.[3] Photolysis of 1,2-c-$C_4F_6Cl_2$, reaction 1, and reactive loss through reactions 2b and 2c lead to the formation of reactive chlorine in the stratosphere and, thus, catalytic ozone destruction.[4]

Quantifying the atmospheric photolysis rate (photolysis lifetime) of (*E*)- and (*Z*)-1,2-c-$C_4F_6Cl_2$ requires knowledge of their UV absorption spectra, particularly over the wavelength range 190 to 230 nm at temperatures relevant to the stratosphere. The UV absorption spectra of (*E*)- and (*Z*)-1,2-c-$C_4F_6Cl_2$ are not currently available in the literature and were measured as part of this study. In addition, photodissociation of R-316c was established via measurements of Cl atom photolysis quantum yields and the formation of the stable hexafluorocyclobutene (c-C_4F_6) co-product in the 193 nm laser photolysis of 1,2-c-$C_4F_6Cl_2$. The total rate coefficient, i.e., $O(^1D)$ loss, and the reactive rate coefficient, i.e., 1,2-c-$C_4F_6Cl_2$ loss, were measured for the $O(^1D)$ + 1,2-c-$C_4F_6Cl_2$ reaction in this work at 296 K. Tropospheric loss processes for 1,2-c-$C_4F_6Cl_2$, such as reaction with OH radicals, Cl atoms, and O_3 are expected to be negligible and upper-limits for the OH and O_3 reaction rate coefficients were determined in this work. Infrared absorption spectra for (*E*)- and (*Z*)-1,2-c-$C_4F_6Cl_2$ were measured to enable an evaluation of their radiative efficiencies and global warming potentials (GWPs).

In this study, key atmospheric loss processes for the (*E*) and (*Z*) isomers of 1,2-c-$C_4F_6Cl_2$ were quantified in a series of independent laboratory measurements as described above. The experimental results were used as input to the Goddard Space Flight Center (GSFC) 2-D atmospheric model[5,6] and a line-by-line radiative transfer model[7] to evaluate local and globally annually averaged atmospheric lifetimes and the ozone depletion and global warming potentials, respectively, which are metrics used in assessments and policy decision making. The present work establishes that the (*E*) and (*Z*) isomers of 1,2-c-$C_4F_6Cl_2$ are long-lived species that are primarily removed in the stratosphere by UV photolysis. As a result of their long lifetimes, the isomers of R-316c are potent ozone depleting substances as well as greenhouse (radiative forcing) gases. This work has also shown that the UV photolysis of (*E*)- and (*Z*)-1,2-c-$C_4F_6Cl_2$ leads to the direct formation of c-C_4F_6 in the stratosphere, which itself is a potent greenhouse gas.

2. EXPERIMENTAL DETAILS

In this study, a number of independent laboratory experiments were performed to quantify key atmospheric removal processes for the (*E*) and (*Z*) isomers of 1,2-c-$C_4F_6Cl_2$ (R-316c). The experiments performed on R-316c included measurements of (1) UV absorption spectra over the wavelength range 184.95−230 nm at temperatures between 214 and 296 K, (2) Cl atom quantum yields following its 193 nm photolysis, (3) c-C_4F_6 product yields following 193 nm photolysis of R-316c, (4) $O(^1D)$ atom total and reactive rate coefficient measurements at 296 K, (5) an upper-limit for the OH radical reaction rate coefficient at 296 K, and (6) an upper-limit for the O_3 reaction rate coefficient at 296 K. In addition, the infrared absorption spectra of (*E*)- and (*Z*)-1,2-c-$C_4F_6Cl_2$ were measured between 500 and 4000 cm^{-1} at 296 K. Experiments were performed using commercial 1,2-c-$C_4F_6Cl_2$ samples consisting of (*E*)/(*Z*) isomeric mixtures with mixing ratios of 0.94/0.06 and 0.475/0.525. The experimental apparatus and methods used in this work have been described in previous studies from this laboratory and are described only briefly below. In the Atmospheric Implications section that follows, the results from this work were used to determine annually averaged local and global atmospheric lifetimes, ozone depletion potentials (ODPs), radiative efficiencies, and global warming potentials (GWPs) for (*E*)- and (*Z*)-1,2-c-$C_4F_6Cl_2$.

2.1. UV Absorption Spectra Measurements. UV absorption spectra of the (*E*)- and (*Z*)-1,2-c-$C_4F_6Cl_2$ samples were measured at discrete wavelengths over the range 184.95−230 nm at 214, 233, 253, 273, and 296 K. The UV absorption spectra of the individual isomers were not measured directly but determined from a linear regression analysis of the measured spectra of the isomerically mixed samples and their mixing ratios. The experimental apparatus has been used in recent studies from this laboratory[8−10] and consisted of a light source, either a 30 W deuterium (D_2) lamp or low-power Hg (184.95 nm), Zn (213.95 nm), or Cd (228.80 nm) atomic lamps, a jacketed Pyrex absorption cell, a 0.25 m monochromator with a photomultiplier tube (PMT) detector used with the D_2 light source, or a photodiode detector used with the atomic light sources. The temperature of the absorption cell was maintained by circulating a temperature-regulated fluid through its outer jacket. The temperature of the gas in the cell was measured at the entrance and exit of the cell with a calibrated thermocouple with an accuracy of ±1 K; there was no measurable temperature gradient over the length of the absorption cell. The wavelength of the monochromator was calibrated using the Hg, Zn, and Cd lamp output to ±0.1 nm, and the measurements were made at a spectral resolution of ∼1 nm (FWHM).

Absorption cross sections, $\sigma(\lambda,T)$, at wavelength λ and temperature T were determined using Beer's law

$$A(\lambda) = -\ln[(I(\lambda) - I_B)/(I_0(\lambda) - I_B)] = \sigma(\lambda, T)L[\text{R-316c}] \quad (I)$$

where A is the absorbance, $I(\lambda)$ and $I_0(\lambda)$ are the measured light intensities with and without R-316c present in the absorption cell, respectively, I_B is the background (dark) signal, L is the absorption path length (90.4 cm), and [R-316c] is the

dx.doi.org/10.1021/jp407823k | J. Phys. Chem. A 2013, 117, 11049−11065

total R-316c concentration. At each wavelength, absorbance was measured over a range of R-316c concentrations and $\sigma(\lambda,T)$ was determined from a linear least-squares fit of A versus [R-316c].

Measurements were performed using the following procedure. $I_0(\lambda)$ was recorded after flushing the absorption cell with He bath gas. $I(\lambda)$ values were measured after the cell was flushed with the 1,2-c-$C_4F_6Cl_2$ sample and then filled to a known pressure. The sample pressure was then changed (either increased or decreased) and another $I(\lambda)$ value measured. At least eight different sample concentrations were used to obtain absorbance values in the range 0.02 and 0.6 when possible. $I(\lambda)$ and $I_0(\lambda)$ signals were recorded for >10 s for each measurement and were averaged in the data analysis; the signals were constant and stable to better than 0.5%. $I_0(\lambda)$ measured at the beginning and the end of an individual set of measurements agreed to within 0.5%. The absorption cross sections measured using different lamp intensities, varied by a factor of 5, agreed to within the measurement precision, better than ∼1%.

1,2-c-$C_4F_6Cl_2$ was added to the absorption cell from dilute mixtures of 1,2-c-$C_4F_6Cl_2$ in He that were prepared manometrically off-line in 12 L Pyrex bulbs. The 1,2-c-$C_4F_6Cl_2$ concentration in the absorption cell (in the range $\sim 5 \times 10^{14}$ to $\sim 5 \times 10^{16}$ molecules cm^{-3}) was determined from absolute pressure measurements and the ideal gas law. The composition of the prepared bulbs was stable over the course of the measurements. Also, measurements performed using bulbs with different mixing ratios yielded consistent cross sections to within the measurement precision. Several measurements that were performed at the longer wavelengths used pure samples of the 0.475/0.525 1,2-c-$C_4F_6Cl_2$ $(E)/(Z)$ isomer mixture. Complementary absorption measurements were also performed at 184.95, 213.95, and 228.80 nm using Hg, Zn, and Cd atomic lamps for the light source, respectively, and similar experimental procedures. Band-pass filters were mounted on the lamp source and the photodiode detector to isolate the atomic lines and minimize exposure of the sample to other lamp wavelengths; no sample loss was observed on the time scale of the measurements.

2.2. Cl Atom Quantum Yield Measurements. Cl atom quantum yields, Φ_{Cl}, following the 193 nm photolysis of 1,2-c-$C_4F_6Cl_2$ were determined using the experimental apparatus and following the data analysis methods used previously and described in detail elsewhere.[11,12] The 0.475/0.525 1,2-c-$C_4F_6Cl_2$ isomeric mixture sample was used in all Φ_{Cl} experiments. Measurements were performed using a technique that combined pulsed laser photolysis (PLP) (ArF excimer laser) with time-resolved atomic resonance fluorescence (RF) detection of Cl atoms. Absolute Cl atom quantum yields were determined relative to a reference compound with a known 193 nm photolysis quantum yield. Oxalyl chloride, $(COCl)_2$, was used as the reference compound; the effective Cl atom yield in the 193 nm photolysis of $(COCl)_2$ was measured previously in our laboratory to be 2 under the conditions of the present experiments.[11]

The photolysis laser beam passed through a 1.5 cm^2 iris before entering the small volume (∼250 cm^3) multiport Pyrex RF reactor. The photolysis laser repetition rate was typically 5 Hz, to ensure a fresh gas sample for each laser pulse. The photolysis beam was monitored at the reactor exit with a calibrated power meter and the laser fluence was varied between 1.4 and 5.0×10^{15} photon cm^{-2} pulse^{-1} over the course of the study. Cl atom fluorescence was detected at a 90° angle to the photolysis beam by a solar-blind photomultiplier tube (PMT). The PMT signal was processed by a 100 MHz amplifier-discriminator and digitized on a 32 bit 80 MHz data acquisition board. Cl atom temporal profiles were recorded for each photolysis laser pulse in 5 μs bins over 30 ms with a typical co-addition of ∼6000 temporal profiles. The background signal was measured for 1 ms prior to the firing of the photolysis laser.

Resonant Cl atom excitation radiation, $^{2,4}P_{1/2} \leftarrow {}^2P_{3/2}$ transitions at 133.57 and 137.31 nm, was produced in a low-pressure (∼2 Torr) microwave discharge lamp with a slow flow of a dilute Cl_2 in He mixture, 0.5%. The VUV excitation radiation entered the reactor through a CaF_2 window orthogonal to the plane defined by the photolysis laser beam and the PMT detector. The Cl atom sensitivity was typically $\sim 2 \times 10^9$ atom cm^{-3} Hz.

The 1,2-c-$C_4F_6Cl_2$ concentration in these experiments was measured online using Fourier transform infrared (FTIR) absorption (described below). The 1,2-c-$C_4F_6Cl_2$ concentration in the RF reactor was in the range $(0.5-7.0) \times 10^{14}$ molecules cm^{-3}. The $(COCl)_2$ concentration was measured prior to the RF reactor in a 100 cm UV absorption cell by absorption at 213.95 nm (Zn line); the absorption cross section used was $(1.72 \pm 0.09) \times 10^{-18}$ cm^2 molecule^{-1}.[11] The gas flow exiting the UV absorption cell was diluted prior to entering the RF reactor, and the $(COCl)_2$ concentration in the RF reactor was varied over the range $(0.4-4.0) \times 10^{14}$ molecules cm^{-3} over the course of the study. SF_6 was added to the reaction mixture, $\sim 5.5 \times 10^{15}$ molecules cm^{-3}, to ensure collisional quenching of spin−orbit excited $Cl(^2P_{1/2})$ atoms produced in the photolysis of $(COCl)_2$. There was no evidence for the formation of $Cl(^2P_{1/2})$ in the photolysis of 1,2-c-$C_4F_6Cl_2$, but SF_6 was maintained in these measurements as well. Cl atom quantum yields were determined from measurements of the Cl atom temporal profiles obtained for a series of 1,2-c-$C_4F_6Cl_2$ and $(COCl)_2$ concentrations; at least five different concentrations were used while the other experimental conditions such as reactor pressure, gas flow rates, photolysis laser fluence, and microwave discharge lamp power were constant.

The loss of Cl atoms following photolytic production was minor and the initial photolysis signal, S_0, was obtained by fitting the observed Cl atom profile to a first-order (exponential) decay between 0.1 and 10 ms. S_0 is proportional to the initial Cl atom concentration, $[Cl]_0$

$$S_0 \propto [Cl]_0 = F\sigma\Phi_{Cl}[R-316c] \quad \text{(II)}$$

where F is the photolysis laser fluence and σ is the effective R-316c isomeric mixture absorption cross section at 193 nm (5.88×10^{-19} cm^2 molecule^{-1}) measured in this work. A similar equation can be written for the $(COCl)_2$ reference compound; the $(COCl)_2$ absorption cross section at 193 nm was taken to be 3.83×10^{-19} cm^2 molecule^{-1}.[13] The R-316c Cl atom quantum yield was obtained relative to the reference compound using the relationship

$$\Phi_{Cl} = \left(\frac{S_0^{R\text{-}316c}}{S_0^{Ref}}\right)\left(\frac{[Ref]}{[R\text{-}316c]}\right)\left(\frac{\sigma_{Ref}}{\sigma_{R\text{-}316c}}\right)\Phi_{Cl}^{Ref} \quad \text{(III)}$$

Linear least-squares fits of the measured S_0 vs [R-316c] and $[(COCl)_2]$ data were used in the data analysis. Differences in Cl atom sensitivity between the sample and reference compound measurements were accounted for in the final data analysis as described elsewhere.[11,12,14]

2.3. Stable Photolysis Products. Stable co-products in the 193 nm pulsed laser photolysis of (E)- and (Z)-R-316c at 296 K were measured by PLP combined with infrared absorption

detection of the stable products. The infrared spectra measured following the static photolysis of R-316c were used to quantify the extent of photolysis of the R-316c isomers by quantitative subtraction of reference spectra. Photolysis of R-316c was performed in a 100 cm long (2.5 cm i.d.) Pyrex reactor while the sample was continuously circulated between the reactor and a low volume, ~500 cm^3, multipass infrared absorption cell. Gases were circulated using a Teflon diaphragm pump. Infrared spectra were measured using FTIR spectroscopy at 1 cm^{-1} resolution over the range 500 to 4000 cm^{-1} with 100 co-adds. The excimer laser beam passed through the length of the reactor and the laser fluence was monitored at the reactor exit. The laser was operated at 5 Hz and the fluence was varied between 1.5 and 3.6 mJ cm^{-2} $pulse^{-1}$ over the course of the experiments.

Experiments were performed at ~640 Torr (He bath gas) total pressure over a range of initial conditions. The primary product yield experiments were conducted with ethane (C_2H_6), $(1.8-9.0) \times 10^{15}$ molecules cm^{-3}, added to the photolysis mixture as a Cl atom scavenger. Additional experiments were performed with O_2 added to the mixture, $\sim 1 \times 10^{18}$ molecules cm^{-3}, or with O_2 as the bath gas. Experiments were performed with both R-316c isomeric mixture samples with initial concentrations in the range $(0.63-1.08) \times 10^{15}$ molecules cm^{-3}.

Experiments were performed by exposing the reaction mixture to a number of laser pulses, typically between 25 and 1000, followed by the measurement of the mixtures infrared absorption spectrum. The number of laser pulses used was gradually increased over the course of an experiment. c-C_4F_6, CF_2O, $(FCO)_2$, and $FC(O)CF_2CF_2C(O)F$ were quantified using reference spectra measured as part of this work. The infrared band strength measured for c-C_4F_6, $(2.22 \pm 0.12) \times 10^{-16}$ cm^2 $molecule^{-1}$ cm^{-1} between 802 and 1543 cm^{-1}, was in good agreement with the value reported by Bravo et al.,[15] to within 3%.

2.4. $O(^1D)$ Rate Coefficient Measurements. The total rate coefficient, k_T, corresponding to $O(^1D)$ loss in the $O(^1D)$ + 1,2-c-$C_4F_6Cl_2$ reaction was measured at 296 K using a competitive reaction method. $O(^1D)$ atoms were produced by PLP, while the total rate coefficient was determined from analysis of the OH radical temporal profile produced from the $O(^1D)$ + n-C_4H_{10} (n-butane) reference reaction that was measured by laser-induced fluorescence (LIF). The reactive rate coefficient, k_R, for the $O(^1D)$ + 1,2-c-$C_4F_6Cl_2$ reaction was measured at 296 K using a relative rate technique with N_2O and CF_2Cl_2 (CFC-12) used as reference compounds. The $O(^1D)$ reaction rate coefficient measurements were performed using the 0.475/0.525 1,2-c-$C_4F_6Cl_2$ isomeric mixture sample. The total and reactive rate coefficient apparatus and methods are described separately below.

2.4.1. $O(^1D)$ Total Rate Coefficient, k_T. The total rate coefficient for the $O(^1D)$ + 1,2-c-$C_4F_6Cl_2$ reaction was measured at 296 K using a competitive reaction technique that measures the temporal loss of the $O(^1D)$ atom. Details of the competitive reaction method and data analysis are provided in previous studies from this laboratory[16−18] and are only briefly described here. In this method, $O(^1D)$ was produced by PLP of O_3 at 248 nm (KrF excimer laser)

$$O_3 + h\nu(248\ nm) \rightarrow O(^1D) + O_2(^1\Delta) \quad (3a)$$

$$\rightarrow O(^3P) + O_2(^3\Sigma) \quad (3b)$$

where $O(^1D)$ is produced with a 90% yield.[19] $O(^1D)$ radicals were converted to OH radicals via reaction with n-C_4H_{10} (n-butane)

$$O(^1D) + n\text{-}C_4H_{10} \rightarrow OH + products \quad (4)$$

and OH temporal profiles were measured using LIF with excitation of the $A^2\Sigma^+(v' = 1) \leftarrow X^2\Pi(v = 0)$ transition at ~282 nm using the frequency doubled output from a pulsed Nd:YAG pumped dye laser. OH fluorescence was collected, passed through a 308 nm band-pass filter (FWHM = 10 nm), and detected using a photomultiplier tube (PMT). The delay time between the photolysis and the probe laser, i.e., the reaction time, was varied over the range 1−5000 μs.

The photolysis laser fluence was monitored with a power meter mounted after the exit of the LIF reactor and was varied between ~3 and 10 mJ cm^{-2} $pulse^{-1}$ over the course of the study. The initial $O(^1D)$ concentration was calculated to be between 2.8 and 21×10^{11} molecules cm^{-3}.

The total rate coefficient for the $O(^1D)$ reaction with 1,2-c-$C_4F_6Cl_2$ was determined from an analysis of the OH radical temporal profiles measured with different 1,2-c-$C_4F_6Cl_2$ concentrations under pseudo-first-order conditions in $O(^1D)$, i.e., $[O(^1D)] \ll [1,2\text{-c-}C_4F_6Cl_2]$. The OH temporal profile is described by a biexponential expression

$$S_{OH}(t) = C[\exp(-k'_{Loss}t) - \exp(-k'_{Rise}t)] \quad (IV)$$

where $S_{OH}(t)$ is the measured fluorescence signal at time t, which is proportional to the total OH radical concentration, C is a constant, and k'_{Rise} and k'_{Loss} are the pseudo-first-order rate coefficients for the formation and loss of the OH radical, respectively. k'_{Rise} is a measure of the pseudo-first-order loss of $O(^1D)$ in the system and is given by

$$k'_{Rise} = k_4[n\text{-}C_4H_{10}] + k_5[O_3] + k'_b + k_T[R\text{-}316c] \quad (V)$$

where k_4 is 4.75×10^{-10} cm^3 $molecule^{-1}$ s^{-1} at 296 K,[16] k_5 is the rate coefficient for the O_3 reaction

$$O(^1D) + O_3 \rightarrow 2O(^3P) + O_2(^1\Sigma) \quad (5a)$$

$$\rightarrow 2O_2(^3\Sigma) \quad (5b)$$

which is 2.4×10^{-10} cm^3 $molecule^{-1}$ s^{-1} ($k_{5a}/k_5 = 0.5$),[19] and k'_b is the pseudo-first-order rate coefficient for background losses of $O(^1D)$ (reaction with background impurities and diffusion out of the detection volume).

The pseudo-first-order loss of OH radicals, k'_{Loss}, was primarily determined by its reaction with n-butane

$$OH + n\text{-}C_4H_{10} \rightarrow H_2O + products \quad (6)$$

where $k_6 = 2.35 \times 10^{-12}$ cm^3 $molecule^{-1}$ s^{-1}[20] and diffusion out of the detection volume. Under the conditions of our experiments k'_{Loss} was typically <50 s^{-1}. The n-butane concentration was constant during an individual measurement but varied over the range $(2.2-4.0) \times 10^{13}$ molecules cm^{-3} as determined from the measured gas flows and pressure over the course of the study. The O_3 concentration was $\sim 9 \times 10^{12}$ molecules cm^{-3} from measured gas flows and pressure as well as infrared absorption measured prior to dilution.

Total rate coefficients were determined from a non-linear least-squares analysis of a series of OH temporal profiles measured over a range of R-316c concentrations with constant $[n\text{-}C_4H_{10}]$, $[O_3]$, and total pressure. The 1,2-c-$C_4F_6Cl_2$ concentration in the LIF reactor was varied over the range $(3-18) \times 10^{13}$ molecules cm^{-3} as determined by online infrared absorption measurements as well as the measured gas flows and pressures. The agreement between the two measurement methods was within 2−5% in all experiments. A linear least-squares analysis of k'_{Rise} versus $[1,2\text{-c-}C_4F_6Cl_2]$ yielded

the bimolecular total rate coefficient for the $O(^1D)$ + 1,2-c-$C_4F_6Cl_2$ reaction, k_T.

2.4.2. $O(^1D)$ Reactive Rate Coefficient, k_R. The reactive rate coefficient, k_R, for the $O(^1D)$ + 1,2-c-$C_4F_6Cl_2$ reaction was measured at 296 K using a relative rate method with N_2O and CF_2Cl_2 (CFC-12) used as reference compounds. The experimental apparatus and data analysis methods are described in previous studies from this laboratory[17,18] and are only briefly described here. In the relative rate method k_R is determined relative to the rate coefficient of a well-established reaction by monitoring the loss of R-316c relative to that of a reference compound

$$\ln\left(\frac{[\text{R-316c}]_0}{[\text{R-316c}]_t}\right) = \left(\frac{k_R}{k_{ref}}\right)\ln\left(\frac{[\text{ref}]_0}{[\text{ref}]_t}\right) \quad \text{(VI)}$$

where $[\text{R-316c}]_0$, $[\text{R-316c}]_t$, $[\text{ref}]_0$, and $[\text{ref}]_t$ are the R-316c and reference compound concentrations initially and at time t, respectively, and k_{ref} is the $O(^1D)$ reactive rate coefficient for the reference compound. The analysis assumes that R-316c and the reference compound are lost solely by the same reaction, which in this case is reaction with $O(^1D)$.

The experimental apparatus consisted of a FTIR spectrometer used to monitor the change in R-316c and the reference compound concentrations that was coupled to a 1 L Pyrex reactor. FTIR spectra were recorded at 1 cm^{-1} resolution with 100 coadded scans. A Teflon diaphragm pump (12 L min^{-1}) was used to circulate the gases between the reactor and the FTIR absorption cell (300 cm path length, ~500 cm^3 volume). Reactants were added to the reactor from a gas-handling manifold and the initial pressure in the reactor was typically ~100 Torr with He as the bath gas. The gas mixture was circulated (mixed) until consecutively measured FTIR spectra agreed to better than 0.5%, typically for ~15 min, before starting a kinetic measurement. Initial reactant concentrations were $(4.6-11) \times 10^{14}$ molecules cm^{-3} for R-316c, $(17-31) \times 10^{14}$ molecules cm^{-3} for N_2O, and $\sim 0.5 \times 10^{14}$ molecules cm^{-3} for CF_2Cl_2. O_3 was added to the reactor continuously during an experiment from a ~0.3% O_3 in He mixture. The pressure within the reactor increased over the course of the experiment to a final pressure of ~500 Torr.

$O(^1D)$ radicals were produced by PLP of O_3 at 248 nm, reaction 3. The photolysis laser was operated at 10 Hz and the beam passed through the length of the reactor with a fluence of ~4 mJ cm^{-2} $pulse^{-1}$. The loss of R-316c and the reference compound was quantified at discrete reaction intervals relative to their initial concentration. The spectral regions used to quantify losses were 835–900, 908–931, and 2508–2612 cm^{-1} for 1,2-c-$C_4F_6Cl_2$, CF_2Cl_2, and N_2O, respectively. The spectral subtractions had an estimated uncertainty of ±2%.

k_{ref} for the $O(^1D)$ reaction with N_2O and CF_2Cl_2 were taken to be 1.27×10^{-10} cm^3 $molecule^{-1}$ s^{-1}[19] and 1.19×10^{-10} cm^3 $molecule^{-1}$ s^{-1},[17] respectively. For N_2O, k_{ref} is equal to the total rate coefficient for the $O(^1D)$ + N_2O reaction. For CF_2Cl_2, k_{ref} is the reactive rate coefficient for the $O(^1D)$ + CF_2Cl_2 reaction where the total rate coefficient was taken from Baasandorj et al.[17] and the reactive yield was taken to be 0.76.[21]

2.5. OH and O_3 Reaction Rate Coefficient Measurement. The rate coefficient for the OH + 1,2-c-$C_4F_6Cl_2$ reaction was determined at 296 K using a relative rate method with CHF_3 used as the reference compound. The rate coefficient for the OH + CHF_3 reaction was taken to be $(3.1 \pm 0.47) \times 10^{-16}$ cm^3 $molecule^{-1}$ s^{-1} at 298 K.[19] Experiments were carried out using the same apparatus used in the $O(^1D)$ reactive rate coefficient measurements described earlier. The methods used in this study are also similar to and described in a study of the OH + SO_2F_2 reaction from this laboratory.[22] OH radicals were generated by the reaction

$$O(^1D) + H_2O \rightarrow 2OH \quad (7)$$

with H_2O present in large excess and $O(^1D)$ radicals produced by the 248 nm pulsed laser photolysis of O_3, reaction 3. The H_2O concentration was high and in the range $(5.8-6.1) \times 10^{17}$ molecules cm^{-3} and the R-316c and CHF_3 concentrations were in the range $(2.6-3.0) \times 10^{15}$ molecules cm^{-3} and $(9.6-10) \times 10^{16}$ molecules cm^{-3}, respectively. The losses of R-316c and CHF_3 were monitored by FTIR absorption measurements using absorption features between 870–910 and 1120–1180 cm^{-1}, respectively.

A room temperature rate coefficient for the O_3 + R-316c reaction was measured using the same apparatus used for the OH relative rate coefficient determinations. An absolute rate coefficient was determined by monitoring the loss of R-316c in the presence of a known O_3 concentration with both R-316c and O_3 concentrations monitored by FTIR absorption. Measurements were made with an initial concentration of the 0.475/0.525 R-316c mixture of $\sim 1.6 \times 10^{16}$ molecules cm^{-3}. The O_3 concentration was maintained nearly constant, $\sim 1 \times 10^{16}$ molecules cm^{-3}, over the course of an experiment, which lasted several hours, by periodic additions of the O_3/He mixture to the reactor to account for background losses of O_3. The initial reactor pressure was ~100 Torr and increased to ~400 Torr by the end of the measurement.

2.6. Infrared Absorption Spectra. The infrared absorption spectra of the (*E*)- and (*Z*)-1,2-c-$C_4F_6Cl_2$ isomers were determined in this work at 296 K over the range 500–4000 cm^{-1} using FTIR spectroscopy. Infrared absorption spectra were measured for the two isomeric mixture samples at 0.5 cm^{-1} resolution (500 co-added scans) in a 15 cm long absorption cell. Absorption cross sections and integrated bands strengths were determined using the Beer's law, eq I, with the 1,2-c-$C_4F_6Cl_2$ concentration determined using absolute pressure measurements and the ideal gas law. The R-316c samples were added to the infrared absorption cell from dilute manometrically prepared mixtures in He, with 0.13% and 0.51% mixing ratios for the 0.475/0.525 and 0.94/0.06 mixtures, respectively (total pressures in the range 10 to 100 Torr). At least 6 different concentrations were used in the cross section determination for both the 1,2-c-$C_4F_6Cl_2$ isomeric mixture samples; the concentrations used were in the range $(0.42-2.17) \times 10^{16}$ molecules cm^{-3} (0.475/0.525 mixture) and $(0.85-8.56) \times 10^{16}$ molecules cm^{-3} (0.94/0.06 mixture), respectively. As no isomerically pure 1,2-c-$C_4F_6Cl_2$ samples were available, although a high content (*E*)-R-316c sample was used, spectra for the isomers were determined using the spectra obtained for the two isomeric mixtures and the manufacturer reported 0.94/0.06 mixing ratio of the high content (*E*)-1,2-c-$C_4F_6Cl_2$ sample. Analysis of the infrared spectra yielded an isomeric abundance for the other sample of 0.475 (*E*)- and 0.525 (*Z*)-1,2-c-$C_4F_6Cl_2$ with an estimated uncertainty of 1%.

2.7. Materials. Commercial 1,2-c-$C_4F_6Cl_2$ (99% purity) samples were purified in freeze–pump–thaw cycles and stored in Pyrex vacuum-sealed reservoirs. Gas chromatography–mass spectrometric analysis yielded a 1,2-c-$C_4F_6Cl_2$ sample purity of 99%, with the most likely contaminant being 1,1,4-trichloroheptafluorobutane ($C_4F_7Cl_3$) at a 0.3% total abundance level. Additional peaks in the chromatograph corresponding to ion

fragments of mass-to-charge ratio 69 and 85 comprised approximately 0.7% of the total signal counts; these peaks were unidentified. Two 1,2-c-$C_4F_6Cl_2$ samples with different isomeric (*E*)- and (*Z*)- mixing ratios were used in this study. A high content commercial sample of the (*E*)- isomer with a stated (*E*)/(*Z*) ratio of 0.94/0.06 (determined by ^{19}F NMR analysis) was used in our infrared, UV, and 193 nm photolysis experiments. (*E*)-1,2-c-$C_4F_6Cl_2$ consists of an equilibrium mixture of axial (53.4%) and equatorial (46.6%) conformers that were identified in the measured infrared absorption spectra, but assumed to be equivalent in the kinetic or photochemical studies. A sample with a (*E*)/(*Z*) isomeric mixing ratio of 0.475/0.525 (as determined in this work) was used in all experiments. Dilute mixtures (<0.02) of the 1,2-c-$C_4F_6Cl_2$ samples in a He bath gas were prepared manometrically in 12 L Pyrex bulbs. He (UHP, 99.999%), O_2 (UHP, 99.999%), SF_6 (CP, ≥99.8%), N_2O (UHP, 99.99%), CF_2Cl_2 (10.1 ppm in UHP He), CHF_3 (>99.9%), and C_2H_6 (99.0%) were used as supplied. He diluent was passed through a molecular sieve trap at liquid N_2 temperature prior to entering the RF discharge lamp. Dilute mixtures of $(COCl)_2$ (0.005 and 0.01), Cl_2 (0.5%), and C_2H_6 (1×10^{-4}) in a He bath gas were prepared in 12 L Pyrex bulbs. Mixtures were prepared with an overall accuracy of approximately ±1%. The uncertainties quoted throughout the paper are at the 2σ (95% confidence) level unless stated otherwise.

3. THEORETICAL CALCULATIONS

Results from quantum mechanical molecular structure calculations were used in this study to (1) aid the assignment of the infrared absorption spectra, (2) establish photolysis thresholds, and (3) estimate the endothermicity for the OH + R-316c reaction. Molecular structures and energetics were calculated using density functional theory (DFT) methods. In particular, B3P86 functional[23,24] in conjunction with correlation consistent basis set of double-ζ quality, augmented with diffuse functions (AUG-cc-pVDZ) was employed for the optimization of molecular geometries and the calculation of harmonic vibrational frequencies. Absolute electronic energies for all of the species included in the thermochemical calculations were calculated at the B3P86/AUG-cc-pVTZ (triple-ζ basis set) level of theory using the optimized geometries calculated at B3P86/AUG-cc-pVDZ. B3P86 has been shown to yield reliable bond strengths, to within ±10 kJ mol^{-1}, for halogenated molecules.[25] Calculations were conducted with the Gaussian 03 suite of programs.[26] Restricted wave functions were used for the closed-shell molecules; unrestricted wave functions were used for all open-shell radicals. No imaginary vibrational frequencies were found, verifying that all calculated molecular structures correspond to true potential energy minima at the B3P86/AUG-cc-pVDZ energy surface. The zero-point and thermal energies at 298.15 K were derived using harmonic oscillator and rigid rotor approximations and added to the absolute electronic energies to yield the absolute enthalpies for each species. The optimized molecular structures for the (*E*) and (*Z*) isomers of R-316c as well as the axial and equatorial conformers of the (*E*) isomer are shown in Chart 1.

The optimized geometries and harmonic vibrational frequencies (unscaled) for R-316c and all other species included in this work are given in the Supporting Information (Tables S1 and S2). The optimized geometries are in good agreement with the previous published work of Saladino and Tang[27] using B3LYP/6-311+G(2d,p) and MP2/6-311+G(2d,p) levels of theory, although the optimized parameters in this work, in particular the dihedral angles, are slightly more consistent with experimental values.

Chart 1. Optimized Molecular Structures for the (*E*) and (*Z*) Isomers of R-316c as Well as the Axial and Equatorial Conformers of the (*E*) Isomer

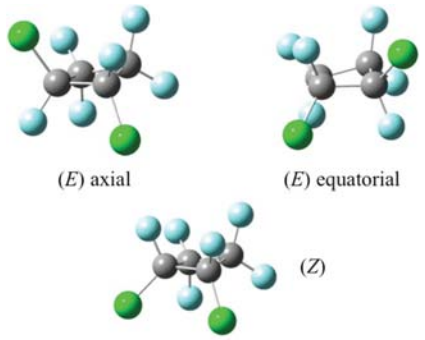

Molecular structures

Regarding the energetics, the axial conformer of (*E*)-1,2-c-$C_4F_6Cl_2$ was calculated to be 0.61 kJ mol^{-1} lower in enthalpy (ΔG = −0.339 kJ mol^{-1} for equatorial ↔ axial) than the equatorial conformer. The (*Z*)-1,2-c-$C_4F_6Cl_2$ stereoisomer was calculated to be 2.98 kJ mol^{-1} higher in enthalpy than the (*E*)-1,2-c-$C_4F_6Cl_2$ axial conformer at 296 K (ΔG = 2.915 kJ mol^{-1} for (*Z*)-R-316c ↔ (*E*)-R-316c (axial)).

4. RESULTS AND DISCUSSION

In this section, results are presented for our measurements of (1) the infrared absorption spectra of the (*E*)- and (*Z*)-R-316c, (2) the UV absorption spectra of (*E*)- and (*Z*)-R-316c between 184.95 and 230 nm at temperatures between 214 and 296 K, (3) the Cl atom quantum yield in the 193 nm photolysis of R-316c, (4) the identification of the stable end-products following the 193 nm photolysis of (*E*)- and (*Z*)-R-316c, (5) rate coefficients for the total and reactive rate coefficient for the O(^{1}D) + R-316c reaction at 296 K, (6) and upper-limit rate coefficients for the OH + R-316c and O_3 + R-316c reactions at 296 K. In addition to the experimental studies, the theoretical calculations described earlier were used to aid the identification of the isomer infrared absorption spectra, establish the photolysis thresholds, and the OH reaction thermochemistry. The experimental results are presented separately below. In the Atmospheric Implications section, the results from our studies are used in a 2-D atmospheric model to evaluate the local and global annually averaged atmospheric lifetimes of R-316c and the relative contributions of the photolytic and kinetic loss processes. On the basis of the calculated lifetimes, ozone depletion potentials (ODPs) and global warming potentials (GWPs) for (*E*)- and (*Z*)-R-316c are presented.

4.1. Infrared Absorption Spectra. Infrared absorption spectra of the 1,2-c-$C_4F_6Cl_2$ isomeric mixture samples were measured at 296 K using FTIR spectroscopy with a spectral resolution of 0.5 cm^{-1}. The measured spectra obeyed Beer's law, ±1% precision, and were independent of total pressure over the range 10−100 Torr (He). The infrared spectra of the (*E*) and (*Z*) isomers were obtained from an analysis of the measured isomeric mixture spectra. The spectra of the isomers are similar, but not identical, which allowed a quantitative identification of the individual spectra using unique absorption features in the (*E*) isomer spectrum. The analysis yielded a (*E*)/(*Z*) isomer mixing ratio of 0.475/0.525 for the unknown sample. Note that this result was used in the interpretation of the UV absorption spectra given below. Figure 1 shows the (*E*) and (*Z*) isomer infrared

dx.doi.org/10.1021/jp407823k | J. Phys. Chem. A 2013, 117, 11049−11065

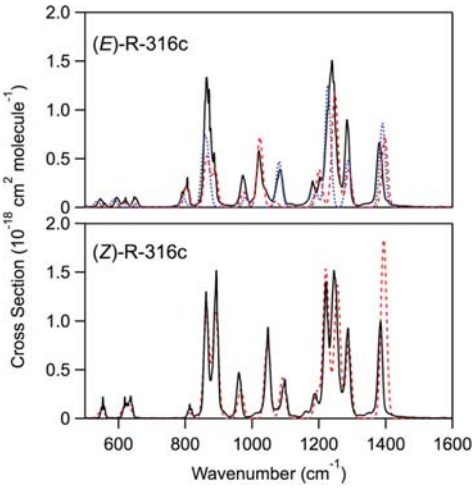

Figure 1. Infrared spectra of (*E*)- and (*Z*)-1,2-dichlorohexafluorocyclobutane (1,2-c-$C_4F_6Cl_2$, R-316c): Solid lines are experimentally determined spectra; dashed and dotted lines are from theoretical calculations in this work (see text). For (*E*)-R-316c, the calculated spectra of the equatorial (dotted blue line) and axial (dashed red line) conformers with 0.466 and 0.534 abundances, respectively, are shown.

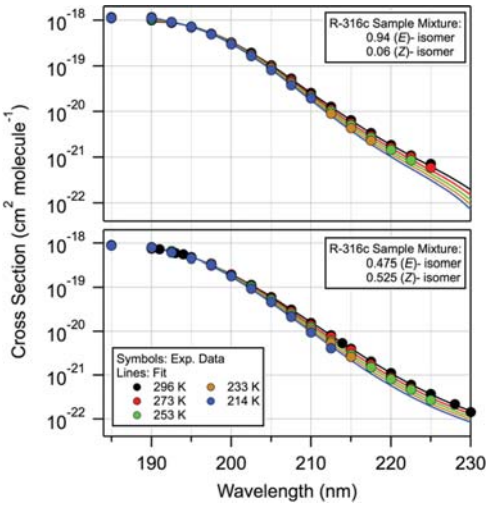

Figure 2. Gas-phase UV absorption spectra (symbols) measured for 0.94/0.06 and 0.475/0.525 (*E*) and (*Z*) isomeric mixtures of 1,2-c-$C_4F_6Cl_2$ (R-316c) over the temperature range 214 to 296 K (see legend). The cross section data is given in Tables S3 and S4 in the Supporting Information. The lines are fits to the data using eq VII.

absorption spectra determined in this work between 500−1600 cm^{-1}. Both spectra show strong absorption in the atmospheric window region, which is characteristic of highly fluorinated compounds, with a peak cross section for (*E*)-1,2-c-$C_4F_6Cl_2$ at 1239.5 cm^{-1} of $(1.51 \pm 0.02) \times 10^{-18}$ cm^2 $molecule^{-1}$. The integrated band strength (IBS) over the range 500−1600 cm^{-1} were measured to be $(1.68 \pm 0.03) \times 10^{-16}$ and $(1.92 \pm 0.05) \times 10^{-16}$ cm^2 $molecule^{-1}$ cm^{-1} for (*E*)- and (*Z*)-1,2-c-$C_4F_6Cl_2$, respectively, where the quoted absolute uncertainties include estimated systematic errors. The infrared spectra of (*E*)- and (*Z*)-1,2-c-$C_4F_6Cl_2$ are provided in digital form in the Supporting Information.

Figure 1 includes the infrared spectra calculated theoretically in this work. The agreement with the experimental spectra is, in general, very good for Gaussian band shapes with full width at half maxima of ∼20 cm^{-1} for all bands as shown in Figure 1. The infrared spectra for the equatorial and axial conformers of (*E*)-R-316c are included in Figure 1 taking the axial (53.4%) and equatorial (46.6%) conformer distribution calculated theoretically in this work. Saladino and Tang[27] report a calculated axial (41.3%) equatorial (58.7%) distribution, which differs but falls within the combined overall uncertainties of the calculations.

4.2. UV Absorption Spectra. The UV absorption spectra, $\sigma(\lambda,T)$, of the 1,2-c-$C_4F_6Cl_2$ (R-316c) samples were measured at discrete wavelengths over the range 184.95 to 230 nm. Measurements were made at 214, 233, 253, 273, and 296 K for the 0.475/0.525 and 0.94/0.06 (*E*)/(*Z*) isomer mixtures and the results are summarized in Tables S3 and S4 of the Supporting Information. Figure 2 shows the experimentally measured spectra of the isomer mixtures. The absorption cross sections decrease monotonically with increasing wavelength between 190 and 230 nm; the cross section values for the mixtures decrease by nearly 4 orders of magnitude from a maximum of $\sim 8 \times 10^{-19}$ cm^2 $molecule^{-1}$ at 190 nm. A qualitative comparison of the spectra shown in Figure 2 indicates that the (*E*) and (*Z*) isomers have significantly different absorption spectra over the wavelength range of the measurements, i.e., the measured spectra are dependent on the isomeric mixing ratio. It is also evident from these spectra that the (*E*)-R316c isomer absorption cross sections are greater than that of the (*Z*)-R-316c isomer over this wavelength range.

A dependence of the measured absorption spectra on temperature was observed (see Tables S3 and S4 and Figure 2) with decreasing cross section values measured at all wavelengths with decreasing temperature. The observed temperature dependence was greatest at the longest wavelengths. For example, the change in σ(200 nm,T) between 296 and 214 K was measured to be ∼10%, while a ∼39% change was observed at 210 nm for the (*E*) isomer.

The UV absorption spectra were measured over a range of experimental conditions including variations in the range of absorption, light source intensity, and sample bulb mixing ratio. In all cases, the measured absorption varied linearly with [1,2-c-$C_4F_6Cl_2$], i.e., obeyed Beer's law. The precision of the measurements was high, particularly in the wavelength range most relevant for atmospheric photolysis, 200 to 220 nm, while the uncertainty increased slightly at longer wavelengths due primarily to the weak 1,2-c-$C_4F_6Cl_2$ absorption. In most cases, three to four separate sets of measurements were performed at each wavelength and temperature. The measured $\sigma(\lambda,T)$ values agreed to within the measurement precision, ∼2%. The data reproducibility was also tested extensively by performing measurements with variations of the optical filtering, lamp intensity, and monochromator resolution (varied from 1 to 2 nm), which also yielded $\sigma(\lambda,T)$ results that agreed to within the measurement precision. Measuring the UV absorption spectrum of N_2O at room temperature and wavelengths between 184.95 and 250 nm further validated the experimental methods.[9] The $\sigma(\lambda,T)$ values given in Tables S3 and S4 were obtained from an average of all of the measurements performed at a given wavelength and temperature. The 2σ uncertainties reported in Tables S3 and S4 are from the measurement precision and encompass the extremes of the individual measurements.

The UV spectra of the (*E*)- and (*Z*)-R-316c isomers were obtained from a linear regression of the experimental

dx.doi.org/10.1021/jp407823k | J. Phys. Chem. A 2013, 117, 11049−11065

data using fits of the experimental data to the empirical expression

$$\log_{10}(\sigma(\lambda, T)) = \sum_i A_i(\lambda - 200)^i + (296 - T)\sum_i B_i(\lambda - 200)^i \quad \text{(VII)}$$

and the isomeric sample mixing ratios reported for the 0.94/0.06 sample and determined in this work for the 0.475/0.525 sample. The fits reproduced the experimental data to better than 3%. The wavelength and temperature dependent UV absorption spectra of (*E*)- and (Z)-1,2-c-$C_4F_6Cl_2$ were parametrized for use in atmospheric models using eq VII. The fit parameters are given in Tables 1 and 2, and the spectra calculated for the temperatures included in this work are displayed in Figure 3. The parametrization is valid over the range of the experimental data; extrapolation to lower temperatures and outside the wavelength range of the measurements may lead to less reliable results. The obtained (*E*)-R-316c spectrum is nearly identical to the spectrum measured for the 0.94/0.06 (*E*)/(*Z*) isomer mixture sample due to the (*E*)- isomer being a stronger absorber in this wavelength region and that the mixture was of high (*E*) isomer content.

The shaded regions in Figure 3 are the estimated uncertainty ranges in the (*E*) and (*Z*) isomer room temperature spectra that include the propagated errors from the two mixture spectra used to determine the pure (*E*) and (*Z*) isomer spectra as well as the uncertainties in the sample isomeric mixing ratios. The estimated uncertainty in the (*E*) isomer room temperature spectrum is ~8% at all wavelengths. The uncertainty in the weaker (*Z*) isomer spectrum is greater, e.g. 12% at 190 nm and 26% at 210 nm. A sample with a higher (*Z*) isomer content would be needed to reduce the level of uncertainty in its UV spectrum using the present methods.

Table 1. Absorption Spectrum, $\sigma(\lambda,T)$, Parameterization for (*E*)-1,2-c-$C_4F_6Cl_2$ (R-316c, 1,2- dichlorohexafluorocyclobutane) That Is Valid over the 190−225 nm Wavelength Range and 210−296 K Temperature Range (see Figure 3)

$$\log_{10}(\sigma(\lambda, T)) = \sum_i A_i(\lambda - 200)^i + (296 - T)\sum_i B_i(\lambda - 200)^i$$

i	A_i	B_i
0	−18.45	−0.000553
1	−0.0876	-8.036×10^{-5}
2	−0.003737	-4.24×10^{-6}
3	0.0001124	-6.01×10^{-7}
4	2.444×10^{-6}	6.00×10^{-8}
5	-9.33×10^{-8}	-1.279×10^{-9}

Table 2. Absorption Spectrum, $\sigma(\lambda,T)$, Parameterization for (*Z*)-1,2-c-$C_4F_6Cl_2$ (R-316c, 1,2- dichlorohexafluorocyclobutane) That Is Valid Over the 190−220 nm Wavelength Range and 210−296 K Temperature Range (see Figure 3)

$$\log_{10}(\sigma(\lambda, T)) = \sum_i A_i(\lambda - 200)^i + (296 - T)\sum_i B_i(\lambda - 200)^i$$

i	A_i	B_i
0	−19.24	−0.00155
1	−0.1037	−0.000761
2	0.00203	-1.22×10^{-5}
3	4.9656×10^{-6}	5.52×10^{-6}
4	-1.65×10^{-5}	-2.365×10^{-7}
5	5.03×10^{-7}	3.33×10^{-9}

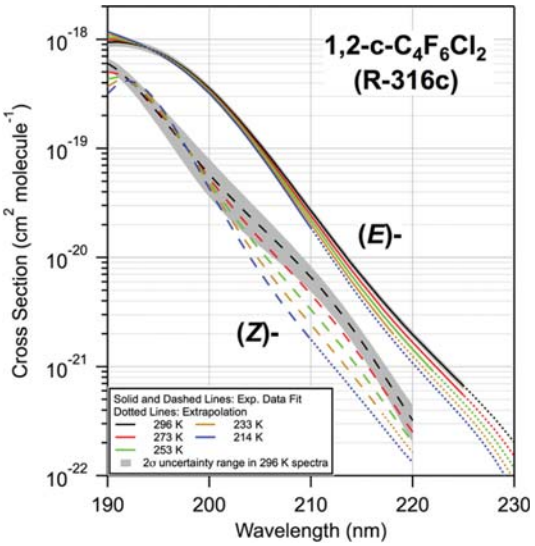

Figure 3. UV spectra of the (*E*) and (*Z*) isomers of 1,2-c-$C_4F_6Cl_2$ UV (R-316c) obtained in this work over the temperature range 214 to 296 K (see legend). The lines were obtained from a linear-regression of the experimental data shown in Figure 2 and were calculated using the cross section parametrization given in Tables 1 and 2. The shaded regions are the estimated 2σ uncertainty ranges for the 296 K spectra (see text for details). The uncertainties for the spectra at the other temperatures displayed are similar but are not shown for improved clarity.

The (*Z*)-R-316c spectrum exhibits a stronger dependence on temperature than observed for the (*E*)-R-316c isomer when compared at the same wavelength. This results from an apparent "blue" shift of the (*Z*)-R-316c absorption spectrum by ~6 nm and the greater sensitivity of the absorption spectrum "tail" to temperature. A blue shift of the (*Z*)-R-316c spectrum implies a higher excitation energy for the (*Z*)- isomer.

The UV absorption spectrum of (*Z*)-R-316c is similar in wavelength dependence and absolute cross section to the UV spectra of the dichlorinated chlorofluorocarbon CF_2Cl_2 (CFC-12) but much greater than that of CF_2ClCF_2Cl (CFC-114) where the chlorine atoms are on different carbon atoms as in R-316c. The cyclic geometry of R-316c, therefore, seems to have an influence on the excitation energy.

4.3. Photolysis Quantum Yields and Stable End-Products. *4.3.1. Cl Atom Quantum Yield.* A summary of the experimental conditions and Cl atom quantum yields, Φ_{Cl}, obtained in the 193 nm pulsed laser photolysis of R-316c is given in Table 3. All quantum yield measurements were performed using the 0.475/0.525 isomeric mixture of R-316c. A weighted average of all of the measurements yields a Φ_{Cl} value of 1.90 ± 0.10 where the uncertainty is from the measurement precision. Representative Cl atom temporal profiles obtained for R-316c and $(ClCO)_2$, the reference compound used in this work, are shown in Figure 4. Following the photolysis laser pulse, the Cl atom temporal profile shows an instantaneous jump and a

dx.doi.org/10.1021/jp407823k | J. Phys. Chem. A 2013, 117, 11049−11065

Table 3. Experimental Conditions and Cl Atom Quantum Yields, Φ_{Cl}, Obtained in the 193 nm Photolysis of 1,2-c-$C_4F_6Cl_2$ (R-316c)

pressure (Torr, He)	$[O_2]^a$	photolysis laser fluence^b	$[(COCl)_2]^c$	[R-316c]^{c,d}	$\Phi_{Cl}{}^e$
41		2.9	0.38−1.12	0.47−2.49	1.80 ± 0.14
41		2.6	1.10−2.20	1.81−4.73	1.95 ± 0.26
41		5.0	0.76−1.92	1.95−4.42	2.23 ± 0.36
149		3.8	0.75−1.97	1.56−4.57	2.12 ± 0.32
41	3.54	1.4	1.76−3.96	4.26−7.04	1.78 ± 0.31

^{a}In units of 10^{16} molecules cm^{-3}. ^{b}In units of mJ cm^{-2} pulse^{-1}. ^{c}In units of 10^{14} molecules cm^{-3}. ^{d}Total concentration of isomeric mixture. The mixture was determined in this work to be 0.475 (*E*)- and 0.525 (*Z*)-1,2-c-$C_4F_6Cl_2$. ^{e}The effective quantum yield for the isomeric mixture where the uncertainties are at the 2σ level from the measurement precision.

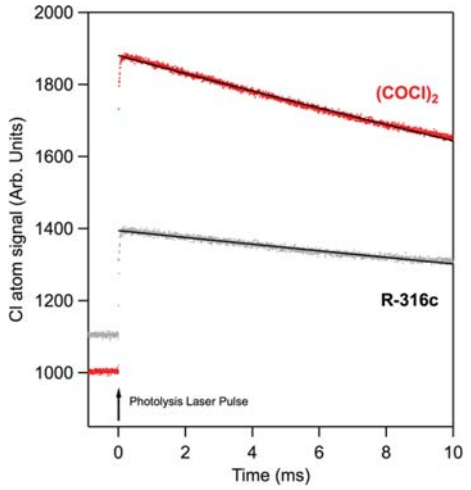

Figure 4. Cl atom temporal profiles measured by atomic resonance fluorescence following the 193 nm pulsed laser photolysis of 1,2-c-$C_4F_6Cl_2$ (R-316c) and $(COCl)_2$ in 41 Torr of He; laser fluence was 2.5 × 10^{15} photon cm^{-2} pulse^{-1} and [R-316c] and $[(COCl)_2]$ were 1.7 × 10^{14} and 1.1 × 10^{14} molecules cm^{-3}, respectively. The arrow indicates the firing of the photolysis laser, t_0. The solid lines are least-squares fits of the data used to determine S_0, eq II.

subsequent slow decay due primarily to Cl atom diffusion out of the detection region (i.e., there was no detectable Cl atom reactive loss in this system); typical decay rate coefficients were <17 s^{-1}. The slow decay in the Cl atom signal enabled an accurate (±~1%) determination of the initial Cl atom signal, S_0.

Φ_{Cl} was independent of pressure over the range 41−149 Torr (He), the photolysis laser fluence, varied between 1.4 and 5.0 × 10^{15} photon cm^{-2} pulse^{-1}, and the addition of 1 Torr O_2, to within the measurement precision. Uncertainty in the concentrations of 1,2-c-$C_4F_6Cl_2$ (±6%) and $(COCl)_2$ (±9%) and 193 nm absorption cross sections of 1,2-c-$C_4F_6Cl_2$ (±5%) and $(COCl)_2$ (±5%) contributed to the estimated ~±14% absolute uncertainty in Φ_{Cl}(193 nm), Φ_{Cl}(193 nm) = 1.90 ± 0.27. Note that no distinction between the (*E*) and (*Z*) isomer Cl atom quantum yields was made in the analysis.

A Cl atom quantum yield of ~2 implies a R-316c quantum yield of unity and that both Cl atoms are released from 1,2-c-$C_4F_6Cl_2$ following UV absorption. Photodissociation thresholds were calculated theoretically in this work to be 309.8 kJ mol^{-1} (~386 nm) and 307.4 kJ mol^{-1} (~389 nm) for a single Cl atom elimination from (*E*)- and (*Z*)-R-316c, respectively. For the elimination of both Cl atoms and the formation of c-C_4F_6 (perfluorocyclo-butene) as a co-product the calculated thresholds are 392.8 (~304 nm) kJ mol^{-1} and 390.4 (~306 nm) kJ mol^{-1} for (*E*)- and (*Z*)-R-316c, respectively. The difference in calculated photodissociation thresholds for the axial and equatorial conformers of (*E*)-R-316c were small, <1 kJ mol^{-1}. Therefore, photodissociation of R-316c is energetically allowed at 193 nm and over the wavelength region important for atmospheric photolysis, see Atmospheric Implications section. The identification and quantification of the stable photolysis co-product c-C_4F_6 is described in the next section. An experiment with 3.2 × 10^{16} molecules cm^{-3} of O_2 added to the reaction mixture was performed in an attempt to identify whether the Cl atom elimination was concerted or occurred via a stepwise photodissociation mechanism. O_2 is expected to add to the hexafluorochloroalkyl radical, if formed, to form a stable peroxy radical, where the O_2 + hexafluorochloroalkyl radical rate coefficient is expected to be on the order of ~10^{-12} cm^3 molecule^{-1} s^{-1} (Scheme 1). There was no

Scheme 1. Photolysis and Radical Scavenging

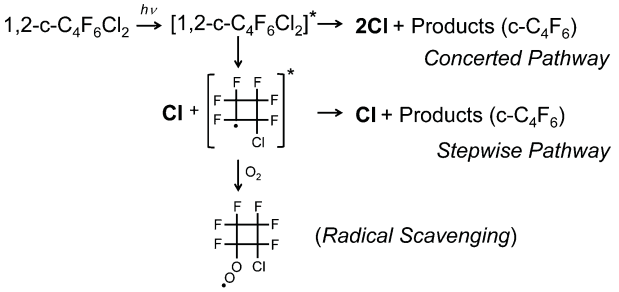

measurable difference in the Cl atom temporal profile or quantum yield in the presence of O_2 to within the measurement precision; that is, the second Cl atom was eliminated on a time scale faster than our measurement time resolution of 5 μs. Higher O_2 concentrations were not used in these measurements due to a significant decrease in Cl atom sensitivity. The Cl atom temporal profiles and quantum yields observed in our experiments, therefore, do not provide clear evidence for the photodissociation mechanism, i.e., either a concerted or sequential photodissociation (see further tests in section 4.3.2).

4.3.2. Stable End-Products. Experiments to measure stable end-product formation following the 193 nm photolysis of R-316c were performed using both isomeric mixture samples. Our primary experiments were performed at 646 Torr (He) with C_2H_6 added (≥1.8 × 10^{15} molecules cm^{-3}) to the reaction mixture as a Cl atom scavenger

$$Cl + C_2H_6 \rightarrow HCl + C_2H_5 \quad (8)$$

where k_8(298 K) = 5.7 × 10^{-11} cm^3 molecule^{-1} s^{-1}.[19] The gas mixture was exposed to multiple photolysis laser pulses, while

dx.doi.org/10.1021/jp407823k | J. Phys. Chem. A 2013, 117, 11049−11065

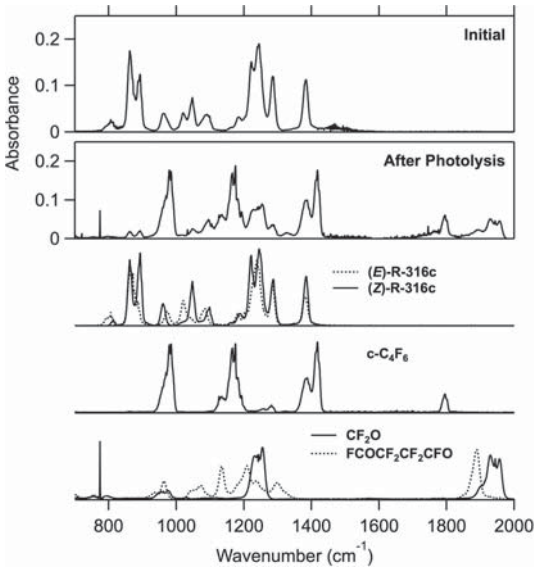

Figure 5. Representative infrared absorption spectra obtained in the determination of stable end-products following the 193 nm pulsed laser photolysis of a (*E*)- and (*Z*)-R-316c and C_2H_6 mixture in 600 Torr He bath gas: initial spectrum with 3.56×10^{14} molecules cm^{-3} and 3.74×10^{14} molecules cm^{-3} of the (*E*) and (*Z*) isomers, respectively, and 1.8×10^{15} molecules cm^{-3} C_2H_6 (top panel); the after photolysis spectrum was obtained following ~6000 photolysis laser pulses (~2 mJ cm^{-2} $pulse^{-1}$). Reference spectra measured in this work and used in the data analysis are shown in the lower panels.

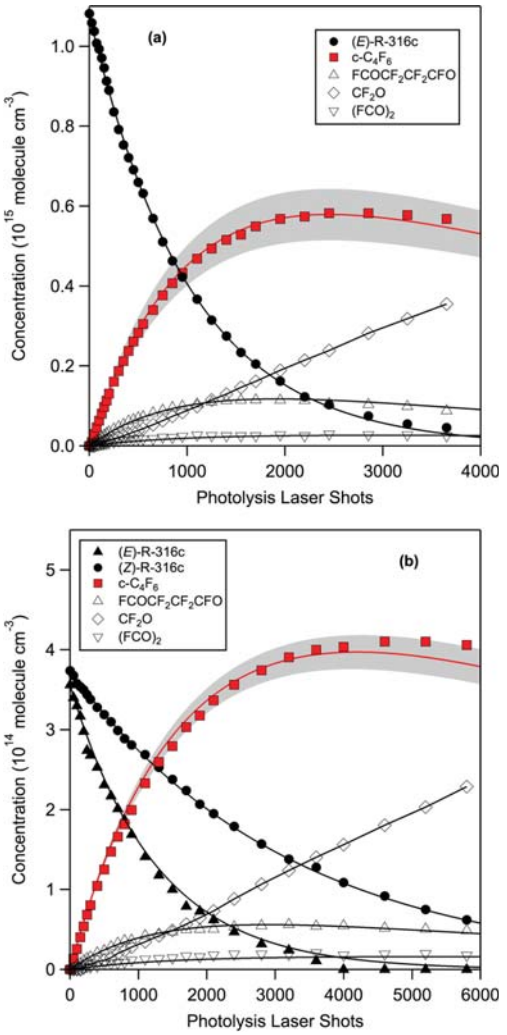

Figure 6. (*E*)- and (*Z*)-R-316c and stable end-product concentration profiles (symbols) measured by infrared absorption following 193 pulsed laser photolysis with the Cl atom scavenger C_2H_6 added. The lines are results from numerical simulations used to determine the product yields (except for CF_2O, see text for details). (a): Photolysis of the 0.94/0.06 (E)-/(Z)- isomeric sample with 1.08×10^{15} molecules cm^{-3} (*E*)-R-316c (the low (*Z*)-R-316c concentration is not shown for clarity), $[C_2H_6] = 1.8 \times 10^{15}$ molecules cm^{-3}, and $[O_2] = 1.2 \times 10^{18}$ molecules cm^{-3}. (b): Photolysis of the 0.475/0.525 (E)-/(Z)- isomeric sample with $[(E)\text{-R-316c}] = 3.56 \times 10^{14}$ molecules cm^{-3}, $[(Z)\text{-R-316c}] = 3.74 \times 10^{14}$ molecules cm^{-3}, and $[C_2H_6] = 1.5 \times 10^{15}$ molecules cm^{-3}. The obtained $c\text{-}C_4F_6$ yields from (*E*)- and (*Z*)-R-316c 193 nm photolysis were 0.72 and 1.0, respectively. The shaded region corresponds to a ± 10% uncertainty range of the $c\text{-}C_4F_6$ yield.

monitoring the loss of (*Z*)- and/or (*E*)-R-316c and the formation of stable end-products by FTIR absorption. Figure 5 shows the infrared spectrum of the initial reaction mixture and the spectrum measured following 5800 photolysis pulses (~2 mJ cm^{-2} $pulse^{-1}$) from a representative experiment with the 0.475/0.525 isomeric mixture. Analysis of the infrared spectra and determination of the $c\text{-}C_4F_6$ product yield was performed using the reference spectra measured in this work shown in the lower panels of Figure 5. The evolution of the reaction mixture composition for this experiment as well as for the photolysis of the 0.96/0.06 isomeric mixture are shown in Figure 6. The R-316c loss over the duration of the experiment was nearly complete for (*E*)-R-316c and >70% for (*Z*)-R-316c; this is due to the greater 193 nm cross section of (*E*)-R-316c. R-316c and the observed products were stable in the apparatus in the absence of photolysis.

A major product observed in the 193 nm photolysis of (*E*)- and (*Z*)-R-316c was $c\text{-}C_4F_6$. CF_2O, CO, and CO_2 and a small concentration of $FC(O)CF_2CF_2CFO$ was also observed. O_2 was not added to the reaction mixture in these experiments, but sufficient O_2 impurity is most likely present to lead to the formation of oxygenated end-products. $c\text{-}C_4F_6$ product yields were obtained by numerical simulation of the observed concentration profiles, e.g. the data given in Figure 6, using a chemical mechanism that accounted for 193 nm photolysis of $c\text{-}C_4F_6$ as well as its reaction with atomic Cl. The 193 nm absorption cross section of $c\text{-}C_4F_6$ was measured in this laboratory to be 1.08×10^{-19} cm^2 $molecule^{-1}$. The observed loss of (*E*)-R-316c was 2.73 times faster than (*Z*)-R-316c, which is consistent with the difference in their 193 nm absorption cross sections; the cross section ratio measured in this work was 2.58. The $c\text{-}C_4F_6$ yields from (*E*)- and (*Z*)-R-316c were found to be 0.72 and 1.0 (±10%), respectively, where the estimated uncertainty represents the range of values that reproduce the experimental data (see Figure 6) reasonably well. The simulations reproduce the formation of $c\text{-}C_4F_6$ at early times, while systematic deviations are observed at longer times. The $c\text{-}C_4F_6$ yield for (*E*)-R-316c was determined from experiments with the 0.94/0.06 sample. Note that reasonable numerical simulations of the $c\text{-}C_4F_6$ profile in the experiment with the 0.475/0.525 (*E*)/(*Z*) isomeric mixture could also be obtained using the upper-limit for the (*E*) isomer yield (~0.82) and a 0.9 yield for the (*Z*) isomer. The obtained yields for the (*E*) and (*Z*) isomers still differ, while the $c\text{-}C_4F_6$ yields for both isomers are high.

dx.doi.org/10.1021/jp407823k | J. Phys. Chem. A 2013, 117, 11049−11065

Table 4. Experimental Conditions and Total Rate Coefficient, k_T, at 296 K for the $O(^1D)$ + 1,2-c-$C_4F_6Cl_2$ Reaction Obtained in This Work Using a Competitive Reaction Technique

pressure (Torr, He)	$[O_3]^a$	$[1,2\text{-c-}C_4F_6Cl_2]^a$	laser fluence (mJ cm^{-2} pulse^{-1})	$[O(^1D)]_0^b$	$[n$-butane$]^a$	k' (10^4 s^{-1})	$k_T{}^c$ (10^{-10} cm^3 molecule^{-1} s^{-1})
50	0.871	4.56–17.9	4.4	4.65	2.21	2.65–4.62	1.57 ± 0.05
50	0.994	3.75–24.9	2.2	2.87	2.79	2.42–6.18	1.54 ± 0.05
100	0.726	3.12–14.9	9.6	21.1	4.02	3.02–5.37	1.61 ± 0.05
50	0.898	3.74–17.9	7.6	12.7	2.61	2.19–5.02	1.56 ± 0.03

[a]In units of 10^{13} molecules cm^{-3}. [b]In units of 10^{11} molecules cm^{-3}. [c]Quoted uncertainties are 2σ from the measurement precision.

The carbon mass balance in these experiments was >90%, while several weak unaccounted for absorption bands were observed.

The temporal behavior and high yields of c-C_4F_6 are consistent with its formation as a primary photolysis product and is also consistent with our measured Cl quantum yield at 193 nm of 1.90 ± 0.27.

$$(E)\text{-R-316c} + h\nu(193\text{ nm}) \rightarrow 2Cl + \text{c-}C_4F_6 \quad \text{yield} = 0.72 \pm 0.07 \qquad (1a)$$

$$\rightarrow 2Cl + \text{products} \qquad (1b)$$

$$(Z)\text{-R-316c} + h\nu(193\text{ nm}) \rightarrow 2Cl + \text{c-}C_4F_6 \quad \text{yield} = 1.0 \pm 0.1 \qquad (1c)$$

$$\rightarrow 2Cl + \text{products} \qquad (1d)$$

The c-C_4F_6 yield in the photolysis of (E)-R-316c is less than unity, which implies that channel 1b is active although the products have not been identified in this study. Channel 1d may also be active within the uncertainty limits of our measurements with a yield up to ~10% possible.

Additional experiments were performed without C_2H_6 added to the photolysis mixture, i.e., no Cl atom scavenger. In these experiments, additional loss of the c-C_4F_6 photolysis product was observed due to the reaction

$$Cl + \text{c-}C_4F_6 \rightarrow \text{products} \qquad (9)$$

where $k_9(298\text{ K}) = 8.88 \times 10^{-13}$ molecule^{-1} cm^3 s^{-1}.[28] The c-C_4F_6 molar yield determined in these experiments was consistent with the results from the scavenger experiments, although less precise due to the loss of c-C_4F_6 via the Cl atom reaction. The carbon mass balance for c-C_4F_6, CF_2O, $FC(O)CF_2CF_2CFO$, and CO in these experiments was ~80% but decreased at longer photolysis times. The lower overall mass balance was attributed to the loss of c-C_4F_6 and the formation of unaccounted for end-products.

An additional photolysis experiment was also performed with the 0.475/0.525 R-316c isomeric mixture in an atmosphere of O_2. This experiment was designed to evaluate the photodissociation mechanism of R-316c further (see section 4.3.1 above). At this high O_2 concentration the pseudo-first-order loss of a hexafluorochlorocycloalkyl radical, if formed, would be ~2×10^7 s^{-1} and possibly lead to different stable end-products. However, the products and yields observed were indistinguishable from those measured in the absence of added O_2. It was, therefore, estimated that the elimination of the second Cl atom occurs on the time scale of 10 ns or less.

4.4. $O(^1D)$ Reaction Rate Coefficients. *4.4.1. Total Rate Coefficient.* The total rate coefficient for the $O(^1D)$ + 1,2-c-$C_4F_6Cl_2$ reaction, reaction 2, was measured at 296 K using the competitive reaction method. Table 4 summarizes the experimental conditions and the rate coefficients obtained in this work at total pressures of 50 and 100 Torr (He); no pressure dependence was observed to within the precision of the measurements. A representative set of measured OH temporal profiles is shown in Figure 7. The profiles show a rapid initial rise in the OH signal

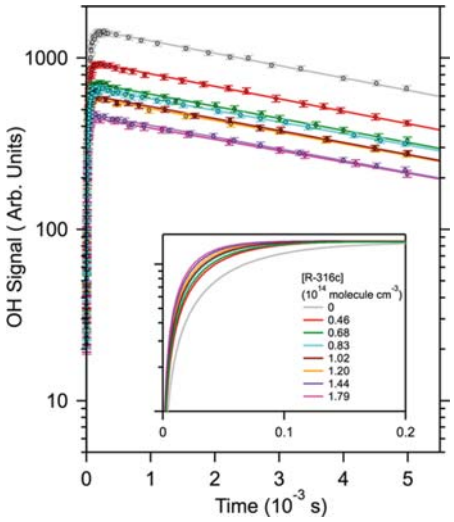

Figure 7. Representative OH temporal profiles obtained in the $O(^1D)$ + 1,2-c-$C_4F_6Cl_2$ (R-316c) reaction experiment at 296 K with the competitive reaction method. The conditions for this experiment were the R-316c concentrations given in the legend, $[n\text{-}C_4H_{10}] = 2.21 \times 10^{13}$ molecules cm^{-3}, $[O_3] = 8.71 \times 10^{12}$ molecules cm^{-3}, 50 Torr (He), and a photolysis laser fluence of 4.4 mJ cm^{-2} pulse^{-1}. The lines are non-linear least-squares fits of the measured OH temporal profiles (symbols). The inset shows the rise region of the non-linear fits, normalized at 1000 μs, more clearly.

followed by a relatively slow decay at longer reaction times. The rate of the initial signal rise increased with increasing 1,2-c-$C_4F_6Cl_2$ concentration, which is shown more clearly in the normalized fits given in the inset in Figure 7. In addition, the total OH production decreased with increasing 1,2-c-$C_4F_6Cl_2$ concentration as reaction 2 does not lead to the formation of an OH radical. The non-linear fits to the OH temporal profiles to eq IV are included in Figure 7 and reproduce the experimental data to within the measurement precision. The $(k'_R - k'_0)$ values from all of the experiments are plotted in Figure 8 versus the 1,2-c-$C_4F_6Cl_2$ concentration. A weighted linear-least-squares fit of the data from each experiment to eq V yielded the $k_T(296\text{ K})$ values given in Table 4. The agreement between the individual experiments was very good and a weighted linear-least-squares fit of the combined data yielded $k_T(296\text{ K}) = (1.56 \pm 0.03) \times 10^{-10}$ cm^3 molecule^{-1} s^{-1}, where the quoted uncertainty is from the fit precision; including estimated systematic errors in the R-316c concentration, ~4%, temperature (1 K) and pressure (1%) measurements, and sample mixing ratios (~2%) yields $k_T(296\text{ K}) = (1.56 \pm 0.11) \times 10^{-10}$ cm^3 molecule^{-1} s^{-1}.

$k_T(296\text{ K})$ measured in this work is consistent with the reported total reactivity of $O(^1D)$ with other chlorinated compounds.

dx.doi.org/10.1021/jp407823k | J. Phys. Chem. A 2013, 117, 11049–11065

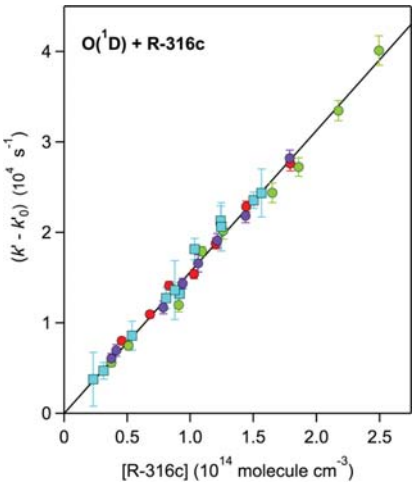

Figure 8. $O(^1D)$ + 1,2-c-$C_4F_6Cl_2$ (R-316c) total rate coefficient data obtained using the competitive reaction method at 296 K and 50 (circles) and 100 Torr (squares). The different symbol colors represent results obtained in independent experiments. The experimental conditions are summarized in Table 4. The error bars on the individual data points are 2σ from the precision of the nonlinear least-squares fits of the OH temporal profiles (e.g., see Figure 7). The line is the linear least-squares fit of all of the data that yields a total rate coefficient of $(1.56 \pm 0.03) \times 10^{-10}$ cm^3 $molecule^{-1}$ s^{-1} where the uncertainty is from the precision of the fit.

For example, the total rate coefficients for $CFCl_3$ (CFC-11), CF_2Cl_2 (CFC-12), and $CFCl_2CF_2Cl$ (CFC-113) are 2.3, 1.4, and 2.0×10^{-10} cm^3 $molecule^{-1}$ s^{-1}, respectively.[19] This implies that the cyclic geometry and the strain of the four member ring of R-316c does not significantly influence the total rate coefficient.

4.4.2. Reactive Rate Coefficient. The reactive rate coefficient for the $O(^1D)$ + 1,2-c-$C_4F_6Cl_2$ reaction, reaction 2, was measured at 296 K using a relative rate method with CF_2Cl_2 (CFC-12) and N_2O used as reference compounds. The experimental data are shown in Figure 9 and a weighted linear least-squares fit of the data to eq VI (forced to a zero intercept) yielded the rate coefficient ratios 1.21 ± 0.02 and 1.01 ± 0.01 for CF_2Cl_2 and N_2O, respectively. The quoted uncertainties are 2σ from the fit precision. For N_2O, the two independent experiments shown in Figure 9 were combined in the final analysis. Taking a reactive rate coefficient for the CF_2Cl_2 reaction of $(1.19 \pm 0.13) \times 10^{-10}$ cm^3 $molecule^{-1}$ s^{-1} from the total rate coefficient reported in Baasandorj et al.[17] and the ClO radical yield (0.76 ± 0.06) for this reaction from Feierabend et al.[21] yields $k_R(296\ K) = (1.44 \pm 0.02) \times 10^{-10}$ cm^3 $molecule^{-1}$ s^{-1}. Taking a reactive rate coefficient for the N_2O reaction of $(1.27 \pm 0.25) \times 10^{-10}$ cm^3 $molecule^{-1}$ s^{-1} from Sander et al.[19] yields $k_R(296\ K) = (1.28 \pm 0.01) \times 10^{-10}$ cm^3 $molecule^{-1}$ s^{-1}. $k_R(296\ K)$ obtained using the two reference compounds are in good agreement with an average value of $(1.36 \pm 0.08) \times 10^{-10}$ cm^3 $molecule^{-1}$ s^{-1}, where the quoted uncertainty is from the measurement precision and does not include the uncertainty in the reference compound rate coefficient (see below). Using $k_T(296\ K)$ measured in this work the reactive yield for the $O(^1D)$ + R-316c reaction is 0.88 ± 0.02 (precision) where the propagated absolute uncertainty is ± 0.20.

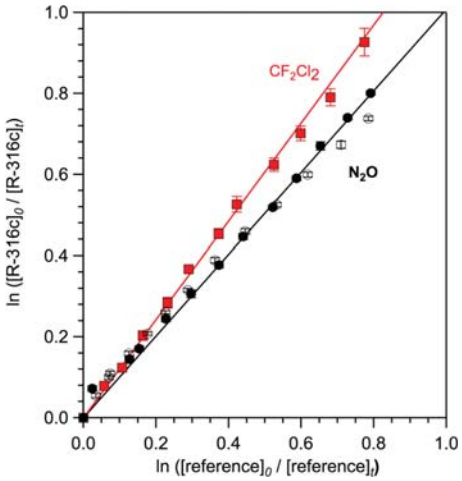

Figure 9. $O(^1D)$ + 1,2-c-$C_4F_6Cl_2$ (R-316c) reactive rate coefficient data obtained at 296 K using a relative rate technique with N_2O (circles) and CF_2Cl_2 (squares) as reference compounds. For N_2O, the filled and open symbols are data obtained in independent experiments. The error bars are at the 2σ confidence level from the precision of the infrared spectral subtraction. Solid lines are weighted linear least-squares fits to the data forced through the intercept.

The precision of the present measurements from the fits shown in Figure 9 was high. The absolute uncertainty in $k_R(296\ K)$ was primarily determined by the absolute uncertainty in the reference compound rate coefficients. Sander et al.[19] estimate the 2σ uncertainty in the $O(^1D) + N_2O$ reaction rate coefficient of 20%. The uncertainty in the reactive rate coefficient for the $O(^1D)$ + CF_2Cl_2 reaction is estimated to be ~12%. The good agreement obtained using the two reference compounds would imply that the overall uncertainties in the reference rate coefficients may actually be less than this. We estimate the absolute uncertainty in $k_R(296\ K)$ for the $O(^1D)$ + R-316c reaction to be ~15%, $k_R(296\ K) = (1.36 \pm 0.20) \times 10^{-10}$ cm^3 $molecule^{-1}$ s^{-1}.

The reactive yield for reaction 2 obtained in this work is consistent with the values reported for other chlorinated compounds.[17,19,21] For example, the reactive yields for $CFCl_3$ (CFC-11), CF_2Cl_2 (CFC-12), and $CFCl_2CF_2Cl$ (CFC-113) are 0.82 ± 0.07,[17] 0.76 ± 0.06,[21] and 0.80 ± 0.10,[16] respectively. Baasandorj et al.[17] estimated that each Cl in a chlorofluorocarbon contributes approximately 0.6×10^{-10} cm^3 $molecule^{-1}$ s^{-1} to the overall reactive rate coefficient. The results from this study are consistent with this estimate, which implies that the cyclic geometry of R-316c does not influence the compound's reactivity with $O(^1D)$ significantly.

During the relative rate experiments infrared absorption features of products formed in reaction 2 were observed; CF_2O, CO_2, and c-C_4F_6 were observed. It is possible that c-C_4F_6 was formed in the unimolecular decomposition of the $\cdot C_4F_6Cl$ radical formed following Cl atom abstraction from R-316c in the $O(^1D)$ reaction

$$\cdot C_4F_6Cl \rightarrow \text{c-}C_4F_6 + Cl \qquad (10)$$

Earlier, we showed that c-C_4F_6 is a primary 193 nm photolysis product of R-316c. Although energetically allowed, the 248 nm absorption cross section of R-316c is much less than 1×10^{-22} cm^2 $molecule^{-1}$ and, therefore, would not contribute to the observed c-C_4F_6 formation. Overall, c-C_4F_6 accounted for only ~3% of the consumed R-316c at the end of the experiment. It is, however, also likely that c-C_4F_6 is lost during the course of the relative rate experiment through reaction with $O(^1D)$ and reaction with Cl atoms generated in the photolysis of R-316c.

4.5. OH and O_3 Rate Coefficient Upper-Limits. The relative rate data obtained in the rate coefficient determination for the OH + R-316c reaction at 296 K are shown in Figure 10.

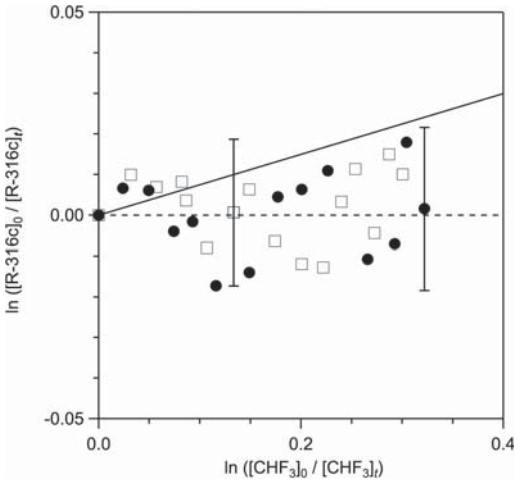

Figure 10. OH + 1,2-c-$C_4F_6Cl_2$ (R-316c) rate coefficient data obtained at 296 K using the relative rate technique with CHF_3 as the reference compound. The different symbols correspond to results obtained in independent experiments. The solid line corresponds to the estimated upper-limit of the rate coefficient ratio reported in this work. The error bars on the data are 2σ from the precision of the infrared spectral subtraction (only shown on two points for improved figure clarity).

The data shows that little, if any, loss of (*E*)- or (*Z*)-R-316c was observed over the course of the experiments, whereas loss of the CHF_3 reference compound was substantial, ~40%. The data points corresponding to a negative loss for R-316c illustrate the range of uncertainty in the infrared spectral subtraction in the data analysis and are not physically meaningful. The overall 1σ uncertainty in the R-316c loss determination was estimated to be ±2%.

A linear least-squares fit of the data in Figure 10 yields a rate coefficient ratio, k_R/k_{ref}, of 0.01 ± 0.02 where the quoted uncertainty is from the precision of the fit. Taking 3.1×10^{-16} cm^3 $molecule^{-1}$ s^{-1} for the OH + CHF_3 reference reaction rate coefficient[19] yields 3.1×10^{-18} cm^3 $molecule^{-1}$ s^{-1} for the OH + R-316c reaction rate coefficient. However, on the basis of the maximum possible measured loss of R-316c a rate coefficient ratio of 0.075 may be possible as shown in Figure 10. This upper-limit yields a rate coefficient upper-limit of 2.3×10^{-17} cm^3 $molecule^{-1}$ s^{-1}, which is our recommended experimental value.

The OH + R-316c reaction rate coefficient upper-limit determined here assumes that 1,2-c-$C_4F_6Cl_2$ and CHF_3 loss was due solely to reaction with the OH radical. However, losses via reaction with O(^{1}D) and 248 nm photolysis are also potential loss processes. On the basis of the UV absorption spectra for the (*E*)- and (*Z*)-1,2-c-$C_4F_6Cl_2$ isomers reported in this work, loss due to 248 nm photolysis of 1,2-c-$C_4F_6Cl_2$ was negligible, whereas CHF_3 does not absorb at 248 nm.[29] Photolytic loss of R-316c and CHF_3 was tested by circulating the reaction mixture for ~2 h with exposure to the photolysis laser, but without O_3 added to the reaction mixture. No reactant loss, <1%, was observed indicating that 248 photolysis was negligible as expected. An additional test was performed with O_3 added to the mixture, with the photolysis laser off, that showed little, <1%, reactant loss. This indicates that ozonolysis, or other dark loss processes, were negligible on the time scale of the present OH relative rate experiments. Loss due to reaction with O(^{1}D) was minimized by maintaining a high H_2O to reactant concentration ratio, $[H_2O] \geq 100$[reactant]. Considering the O(^{1}D) reaction rate coefficients for R-316c as determined in this work and for CHF_3 and H_2O,[19] the O(^{1}D) loss under these conditions due to reaction with R-316c was <1% and <0.05% for CHF_3. A R-316c loss of <1% due to O(^{1}D) reaction was not observable within the precision of our experiments.

The experimentally determined OH + R-316c reaction rate coefficient upper-limit of $<2.3 \times 10^{-17}$ cm^3 $molecule^{-1}$ s^{-1} may actually represent a conservative estimate for this endothermic reaction. A potentially more realistic rate coefficient upper-limit was obtained by assuming the reaction endothermicity to be a lower limit of the reaction activation energy, *E*, with an Arrhenius pre-exponential factor of 1×10^{-11} cm^3 $molecule^{-1}$ s^{-1}, $k = A \exp(-E/RT)$.[3] The reaction endothermicities calculated in this work for Cl atom abstraction, i.e., formation of HOCl as a reaction product, were 72.8 and 72.2 kJ mol^{-1} for axial and equatorial (*E*)-R-316c and 69.8 kJ mol^{-1} for (*Z*)-R-316c. Taking E = 69.8 kJ mol^{-1} yields a room temperature rate coefficient upper-limit of $<5 \times 10^{-24}$ cm^3 $molecule^{-1}$ s^{-1}, which is much less than the experimentally measured upper-limit. Considering the uncertainty in the calculated thermochemistry, an upper-limit rate coefficient of $<3 \times 10^{-22}$ cm^3 $molecule^{-1}$ s^{-1} is possible. Although an OH radical exchange reaction with one of the Cl atoms in R-316c would be exothermic, this reaction pathway is expected to have an extremely high activation barrier and, therefore, is not expected to represent an atmospheric loss process for R-316c. In cases similar to the OH + R-316c reaction where the reaction products and/or the reaction thermochemistry are not well established the estimated rate coefficient upper-limit for the OH + CCl_4 reaction, $<1 \times 10^{-20}$ cm^3 $molecule^{-1}$ s^{-1}, has been assumed in other studies.[3]

As part of this work an upper-limit for the O_3 + R-316c reaction rate coefficient was determined by observing the loss of R-316c in the presence of O_3. Under the conditions described in the experimental section no R-316c loss was observed, <1%, yielding a rate coefficient upper-limit of $<2.0 \times 10^{-22}$ cm^3 $molecule^{-1}$ s^{-1}.

5. ATMOSPHERIC IMPLICATIONS

The experimental results for the UV absorption spectrum and O(^{1}D) reaction rate coefficients were used in the GSFC 2-D atmospheric model to calculate atmospheric loss rates (local lifetimes), their fractional contributions, the global annually averaged lifetimes, and the ozone depletion potentials (ODPs) for (*E*)- and (*Z*)-1,2-c-$C_4F_6Cl_2$ (R-316c). On the basis of the uncertainties in the absorption cross sections and O(^{1}D) rate coefficient, the lifetime uncertainties (ranges) were also evaluated using the 2-D model. The atmospheric lifetimes and the infrared absorption spectra measured in this work were then used to determine the semi-empirical ODPs and global warming potentials (GWPs) for the R-316c isomers.

Details of the GSFC 2-D model are described elsewhere.[5,6] The photolysis rate calculations were separated into contributions from Lyman-α and the 169−190 and 190−230 nm wavelength regions to facilitate a more detailed interpretation of the most critical photolysis regions. The Lyman-α absorption cross sections for the R-316c isomers are unknown, and the $CClF_2CClF_2$ (CFC-114) value (3.6×10^{-17} cm^2 $molecule^{-1}$)[3] was used in the calculations. For wavelengths less than 185 nm where no experimental data are available, the R-316c cross sections were held constant to the 185 nm value. Photolysis rate calculations assume a unit R-316c photolysis quantum yield at all wavelengths. Other model input was taken from Sander et al.[19] and the updates reported in the SPARC lifetime report.[3]

5.1. Atmospheric Lifetimes and Fractional Contributions to Atmospheric Loss. Figures 11 and 12 show the 2-D

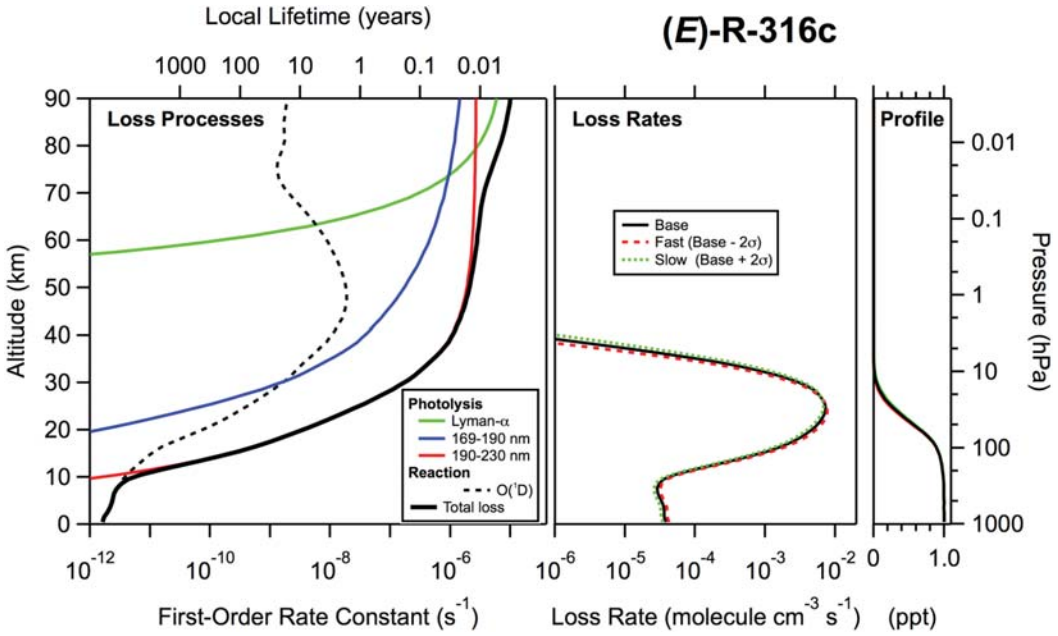

Figure 11. 2-D model results for (*E*)-1,2-c-$C_4F_6Cl_2$ ((*E*)-R-316c). Left: Global annually averaged loss rate coefficient (local lifetime) and photolysis and reaction contributions (see legend). Middle: Molecular loss rate and uncertainty limits; the slow and fast profiles were calculated using the uncertainty estimates for the (*E*)-R-316c absorption spectrum from this work. Right: (*E*)-R-316c concentration profile.

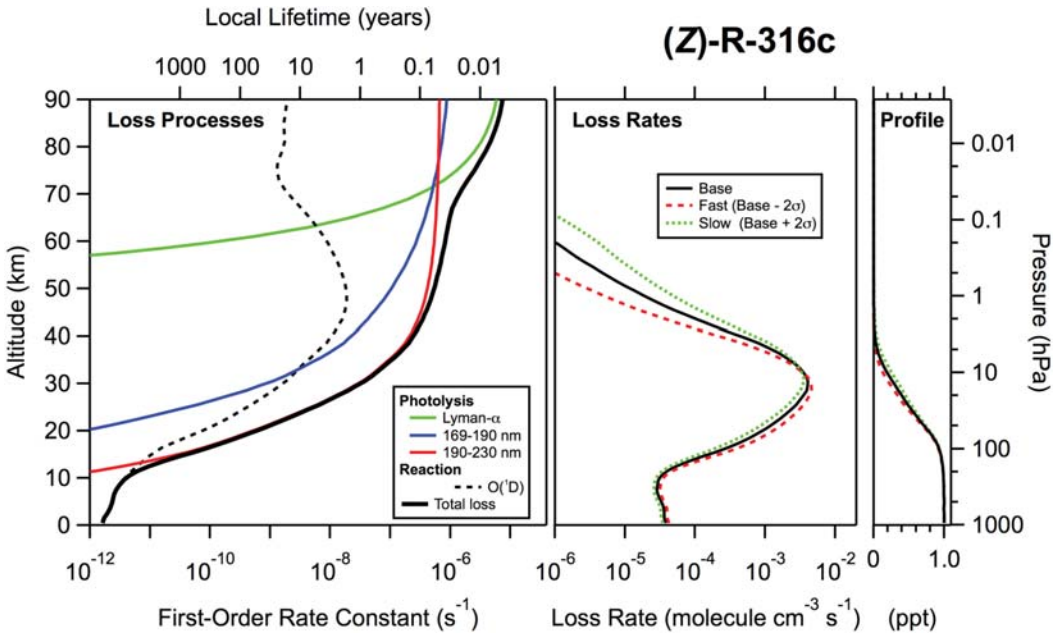

Figure 12. 2-D model results for (*Z*)-1,2-c-$C_4F_6Cl_2$ ((*Z*)-R-316c). Left: Global annually averaged loss rate coefficient (local lifetime) and photolysis and reaction contributions (see legend). Middle: Molecular loss rate and uncertainty limits; the slow and fast profiles were calculated using the uncertainty estimates for the (*Z*)-R-316c absorption spectrum from this work. Right: (*Z*)-R-316c concentration profile.

model calculated total first-order loss rate coefficient (local lifetime) as well as the contributions from the different photolysis regions and the $O(^1D)$ reaction for (*E*)- and (*Z*)-R-316c, respectively. In the upper troposphere and stratosphere, the dominant loss process is photolysis in the 190−230 nm region with minor contributions from the $O(^1D)$ reaction and photolysis in the 169−190 nm region. The UV absorption spectra measured in this work, therefore, included the most critically important wavelength range for atmospheric photolysis.

Also shown in Figures 11 and 12 are the global annually averaged molecular loss rates and the vertical concentration profiles for (*E*)- and (*Z*)-R-316c, respectively. The most critical altitude ranges for atmospheric loss are 18−28 km and 18−35 km for (*E*)- and (*Z*)-R-316c, respectively, where the loss is predominately determined by UV photolysis in the 190−230 nm region. The maximum in the loss rate for (*Z*)-R-316c occurs at a slightly higher altitude because its UV absorption spectrum is weaker than that of (*E*)-R-316c.

dx.doi.org/10.1021/jp407823k | *J. Phys. Chem. A* 2013, 117, 11049−11065

Table 5. Atmospheric Lifetimes and Ranges for (*E*)- and (*Z*)-1,2-$C_4F_6Cl_2$ (R-316c) Calculated Using the GSFC 2-D Model and the Photochemical Parameters Reported in This Work

	(*E*)-1,2-$C_4F_6Cl_2$		(*Z*)-1,2-$C_4F_6Cl_2$	
	lifetime[a] (years)	lifetime range[b] (years)	lifetime[a] (years)	lifetime range[b] (years)
total	74.6	71.7−77.6	114.1	104.6−124.7
tropospheric	3600	3157−4086	10570	9114−11820
stratospheric	76.1	73.4−79.1	115.4	105.7−126.2
mesospheric	$>1 \times 10^6$		98430	384900−35480

[a]Global annually averaged value. [b]Calculated using 2σ upper and lower limits of the UV absorption cross sections reported in this work (see text).

The lifetime was computed as the ratio of the annually averaged global atmospheric burden to the vertically integrated annually averaged total global loss rate.[3] The total global lifetime can be separated by the troposphere (surface to the tropopause, seasonally and latitude-dependent), stratosphere, and mesosphere (<1 hPa) using the total global atmospheric burden and the loss rate integrated over the different atmospheric regions such that

$$\frac{1}{\tau_{Tot}} = \frac{1}{\tau_{Trop}} + \frac{1}{\tau_{Strat}} + \frac{1}{\tau_{Meso}} \quad \text{(VIII)}$$

The global annually averaged lifetimes are 74.6 and 114.1 years for (*E*)- and (*Z*)-R-316c, respectively; that is, both isomers are long-lived ozone depleting substances (Table 5). Since the vast majority of the loss occurs in the stratosphere, the stratospheric lifetimes (76.1 and 115.4 years, respectively) are similar to the total global values. In the troposphere, the loss processes are very weak yielding very long lifetimes (3600 and 10570 years). In the mesosphere, short wavelength UV and Lyman-α photolysis are important local loss processes (Figures 11 and 12, left panels). However, the global mesospheric lifetimes are quite long ($\sim>10^5$ years) since the density weighted loss rates are very small in the mesosphere.

Including the observed spectrum temperature dependence in the 2-D model calculations leads to a lower photolysis rate and, thus, a longer atmospheric lifetime compared to using only the room temperature (296 K) spectrum. This effect was modest, as the total global lifetimes increased from 72.2 to 74.6 years and 106.8 to 114.1 years for (*E*)- and (*Z*)-R-316c, respectively, when including the spectrum temperature dependence. The fractional contributions of the atmospheric loss processes are given in Table 6. The OH + R-316c rate coefficient upper-limit determined in this work results in the OH reaction being a negligible loss process throughout the atmosphere. Lyman-α photolysis only contributes to the local loss in the mesosphere and, therefore, represents a negligible total global atmospheric loss process as well. The dominant loss process is photolysis in the 190−230 nm region with a minor contribution from the 169−190 nm region for (*E*)-R-316c and a greater contribution for (*Z*)-R-316c. The O(^{1}D) reaction accounts for 0.02 of (*E*)-R-316c global loss, whereas it accounts for a much greater fraction of global loss for (*Z*)-R-316c, 0.069.

Table 6. Fractional Losses and Ranges for (*E*)- and (*Z*)-1,2-$C_4F_6Cl_2$ (R-316c) Calculated Using the GSFC 2-D Model and the Photochemical Parameters Reported in This Work

	(*E*)-1,2-$C_4F_6Cl_2$		(*Z*)-1,2-$C_4F_6Cl_2$	
	fractional loss	range	fractional loss	range
	Photolysis Loss			
Lyman-α	0		0	
169−190 nm	0.003	0.003−0.004	0.032	0.019−0.052
190−230 nm	0.977	0.979−0.974	0.899	0.928−0.860
	Reactive Loss			
OH	0		0	
O(^{1}D)	0.020	0.018−0.022	0.069	0.053−0.088

The ranges (uncertainties) in the atmospheric lifetimes and fractional loss contributions were calculated using the 2σ maximum and minimum values of the UV absorption spectra and O(^{1}D) reaction rate coefficient as input to the 2-D model. The uncertainties in the UV absorption cross section data are illustrated in Figure 3 and for the 2-D model calculations were defined as

$$p(T) = p(298\ \text{K}) \exp(|w(1/T - 1/296)|) \quad \text{(IX)}$$

where $p(298\ \text{K})$ is the estimated 2σ uncertainty in the room temperature spectrum and w is a parameter that describes an increase in the uncertainty at other temperatures. In the 2-D model calculation the uncertainty was assumed to be independent of wavelength. The uncertainty parameters used were $p(298\ \text{K}) = 1.08$ and $w = 60$ for (*E*)-R-316c and $p(298\ \text{K}) = 1.3$ and $w = 100$ for (*Z*)-R-316c; only uncertainty in the 190−230 nm wavelength region was included in the calculation. The calculated range in the global lifetimes is given in Table 5. The (*E*)-R-316c lifetime is reasonably well-defined with a spread of ±2.9 years. The lifetime uncertainty for (*Z*)-R-316c is greater, ±10 years, primarily because of the greater uncertainty in its UV absorption spectrum. The corresponding uncertainties in the fractional loss contributions are included in Table 6. It should be noted that, due to uncertainties in other model processes (e.g., transport, O_2, O_3 absorption cross sections), the uncertainty in the absolute lifetime is most likely greater than those obtained due solely to the uncertainty in the model photochemical input parameters.[3]

5.2. Ozone Depletion Potentials. Ozone depletion potentials (ODPs) for (*E*)- and (*Z*)-R-316c calculated using the lifetimes from this work are given in Table 7. ODPs were calculated using a semiempirical method, relative to $CFCl_3$ (CFC-11)

$$\text{ODP}_i = \frac{n_{Cl}}{3} \frac{f_i}{f_{CFC-11}} \frac{\tau_i}{\tau_{CFC-11}} \frac{M_{CFC-11}}{M_i} \quad \text{(X)}$$

In eq X n_{Cl} is the number of Cl atoms in the molecule, f_i is the molecules fractional release factor, and M_i is the molecule's molecular mass. The fractional release factors for (*E*)- and (*Z*)-R-316c have not been evaluated to date. The fractional release factors for $CFCl_2CF_2Cl$ (CFC-113) and CF_2Cl_2 (CFC-12), which have similar lifetimes and atmospheric loss processes, of 0.29 and 0.23 were used for (*E*)- and (*Z*)-R-316c, respectively.[4] f_{CFC-11} was taken from WMO,[4] 0.47. ODPs were also calculated using the 2-D model, following the methodology used previously.[30,31] For this, present

dx.doi.org/10.1021/jp407823k | J. Phys. Chem. A 2013, 117, 11049−11065

Table 7. Lifetimes, Ozone Depletion Potentials (ODPs), and Global Warming Potential (GWPs) for (*E*)- and (*Z*)-1,2-c-$C_4F_6Cl_2$ (R-316c) From This Work

molecule	lifetime[b] (years)	ozone depletion potential (ODP)		radiative efficiency[a] (W m^{-2} ppb^{-1})	global warming potential[c] time horizons (years)		
		semiempirical	2-D model		20	100	500
(*E*)-1,2-c-$C_4F_6Cl_2$	74.6	0.40	0.46	0.27	4660	4160	1710
(*Z*)-1,2-c-$C_4F_6Cl_2$	114.1	0.49	0.54	0.29	5240	5400	2780

[a]Calculated using the infrared spectra measured in this work and a line-by-line radiative transfer calculation. [b]Lifetime based on atmospheric loss due to UV photolysis and reaction with $O(^1D)$ (see text). [c]Referenced to CO_2.

day steady-state simulations were run in which the surface boundary conditions for (1) CFC-11 and (2) R-316c were increased by ~180 ppt to obtain a ~1% depletion in annually averaged global total ozone. It was assumed that each R-316c molecule releases two Cl atoms. The ODP was then calculated as the change in global ozone per unit mass emission of R-316c relative to the change in global ozone per unit mass emission of CFC-11. The calculations were done separately for each R-316c isomer.

The ODPs for (*E*)- and (*Z*)-1,2-c-$C_4F_6Cl_2$ (R-316c) given in Table 7 clearly indicate that both long-lived isomers are potent ozone depleting substances (ODSs). The 2-D model calculated ODPs are ~15 and ~10% greater than estimated using the semi-empirical approach for (*E*)- and (*Z*)-R-316c, respectively. This is reasonable agreement considering that the assumed fractional release factors were taken from other molecules and have a general level of uncertainty due to the overall uncertainty in the stratospheric loss rates of a molecule. The ODP for (*Z*)-R-316c is greater than for (*E*)-R-316c due primarily to its longer atmospheric lifetime.

5.3. Radiative Efficiencies and Global Warming Potentials. Radiative efficiencies (REs) and global warming potentials (GWPs) for (*E*)- and (*Z*)-R-316c were calculated using the infrared absorption spectra (Figure 1) and atmospheric lifetimes (Table 5) from this work. The obtained REs and GWPs are given in Table 7. 1,2-c-$C_4F_6Cl_2$ has several strong vibrational bands that fall within the atmospheric "window", making 1,2-c-$C_4F_6Cl_2$ a potent greenhouse gas. Radiative efficiencies were calculated using an accurate line-by-line (LBL) radiative transfer code[7] and the obtained values agree well with an estimation method developed by Pinnock et al.,[32] which for diffuse absorption bands, as in the present case, has an estimated uncertainty of ~10−15%. The (*E*)- and (*Z*)-R-316c GWPs on the 100-year time horizon are 4160 and 5400, respectively, and are comparable with other long-lived chlorofluorcarbons (CFCs) and hydrofluorocarbons (HFC) with similar lifetimes; that is, their radiative efficiencies are similar. For example, the 100-year time horizon GWPs for $CFCl_2CF_2Cl$ (CFC-113) and CF_2Cl_2 (CFC-12) are 6130 and 10890, respectively, whereas the GWP for CH_3CF_3 (HFC-143a), an HFC with a 52 year lifetime, is 4470.[4]

6. CONCLUSIONS

The atmospheric processing and environmental impact of (*E*)- and (*Z*)-R-316c were evaluated in this work based on a combination of laboratory and 2-D atmospheric modeling studies. R-316c is a chlorofluorocarbon (CFC) of interest, as it is not currently regulated under the Montreal Protocol. In this study the UV absorption spectra, photolysis products, and $O(^1D)$ reaction rate coefficients of the (*E*)- and (*Z*)-R-316c isomers were measured in this laboratory. In addition, rate coefficient upper-limits were measured for the reaction of R-316c with the OH radical and O_3. The results from the laboratory studies were used in a 2-D atmospheric model to calculate annually averaged local and global lifetimes and associated uncertainties. Stratospheric UV photolysis in the 190 to 230 nm wavelength region was shown to be the predominant atmospheric loss process for both isomers of R-316c. Both isomers were also shown to be long-lived ozone depleting substances (ODSs) with global lifetimes of 74.6 ± 2.9 and 114.1 ± 10 years for (*E*)- and (*Z*)-R-316c, respectively; the lifetime uncertainties (ranges) were determined using the 2σ uncertainties in the UV absorption spectra reported in this work. R-316c is an example where the stereoisomer geometry significantly impacts the atmospheric lifetime. For R-316c, the difference in stereoisomer lifetime is primarily due to differences in UV absorption spectra, whereas isomers for other molecules may exhibit differences in reactivity that lead to differences in atmospheric lifetimes. In general, the reactivity and photochemistry of isomers need to be evaluated on a case-by-case basis. The semi-empirical and 2-D model calculations presented in this work have shown that both R-316c isomers have significant ozone depletion potentials (ODPs) of ~0.5. Infrared absorption spectra measured as part of this work were combined with the calculated lifetimes to establish that both isomers of R-316c are also potent greenhouse gases with 100-year time horizon global warming potentials (GWPs) of 4160 and 5400 for the (*E*) and (*Z*) isomers, respectively.

In summary, the chlorofluorocarbons (CFCs) (*E*)- and (*Z*)-1,2-c-$C_4F_6Cl_2$ (R-316c) are atmospherically long-lived ODSs that have substantial ozone depletion potentials (ODPs) and are also potent greenhouse gases. The results from this study will be useful in any future policy decisions regarding the use of R-316c. As a stable end-product of R-316c atmospheric loss, c-C_4F_6 is a potent GHG and, therefore, may also have an impact on the atmosphere. This requires further study.

■ ASSOCIATED CONTENT

Supporting Information

Digitized infrared absorption cross section data for (*E*)- and (*Z*)-R-316c; calculated molecular structure parameters; calculated infrared band positions and intensities for (*E*)- and (*Z*)-R316c; measured UV absorption cross section data for (*E*)/(*Z*) mixtures. This material is available free of charge via the Internet at http://pubs.acs.org.

■ AUTHOR INFORMATION

Corresponding Author

*E-mail: James.B.Burkholder@noaa.gov.

Notes

The authors declare no competing financial interest.

■ ACKNOWLEDGMENTS

This work was supported in part by NOAAs Climate Goal and NASAs Atmospheric Composition: Laboratory Studies and Modeling and Analysis Programs.

REFERENCES

(1) Perouansky, M.; Hentschke, H.; Perkins, M.; Pearce, R. A. Amnesic Concentrations of the Nonimmobilizer 1,2-Dichlorohexafluorocyclobutane (F6, 2N) and Isoflurane Alter Hippocampal θ Oscillations In Vivo. *Anesthesiology* **2007**, *106*, 1168−1176.

(2) Koblin, D. D.; Chortkoff, B. S.; Laster, M. J.; Eger, E. I. N.; Halsey, M. J.; Ionescu, P. Polyhalogenated and Perfluorinated Compounds that Disobey the Meyer-Overton Hypothesis. *Anesth. Analg. (Hagerstown, MD, U. S.)* **1994**, *79*, 1043−1048.

(3) SPARC (2013), SPARC Report on the Lifetimes of Stratospheric Ozone-Depleting Substances, Their Replacements, and Related Species, Ko, M., Newman, P., Reimann, S., Strahan, S., Eds.; SPARC Report No. 6, WCRP-15/2013, 2013.

(4) WMO (World Meteorological Organization), Scientific Assessment of Ozone Depletion: 2010, Global Ozone Research and Monitoring Project-Report No. 52, 516 pp., Geneva, Switzerland, 2011.

(5) Fleming, E. L.; Jackman, C. H.; Stolarski, R. S.; Douglas, A. R. A Model Study of the Impact of Source Gas Changes on the Stratosphere for 1850−2100. *Atmos. Chem. Phys.* **2011**, *11*, 8515−8541.

(6) Fleming, E. L.; Jackman, C. H.; Weisenstein, D. K.; Ko, M. K. W. The Impact of Interannual Variability on Multidecadal Total Ozone Simulations. *J. Geophys. Res.* **2007**, *112*, D10310.

(7) Portmann, R. W.; Solomon, S. Indirect Radiative Forcing of the Ozone Layer During the 21st Century. *Geophys. Res. Lett.* **2007**, *34*, L02813.

(8) Carlon, N. R.; Papanastasiou, D. K.; Fleming, E. L.; Jackman, C. H.; Newman, P. A.; Burkholder, J. B. UV Absorption Cross Sections of Nitrous Oxide (N_2O) and Carbon Tetrachloride (CCl_4) Between 210 and 350 K and the Atmospheric Implications. *Atmos. Chem. Phys.* **2010**, *10*, 6137−6149.

(9) Papadimitriou, V. C.; McGillen, M. R.; Fleming, E. L.; Jackman, C. H.; Burkholder, J. B. NF_3: UV Absorption Spectrum Temperature Dependence and the Atmospheric and Climate Forcing Implications. *Geophys. Res. Lett.* **2013**, *40*, 440−445.

(10) McGillen, M. R.; Fleming, E. L.; Jackman, C. H.; Burkholder, J. B. $CFCl_3$ (CFC-11): UV Absorption Spectrum Temperature Dependence Measurements and the Impact on Atmospheric Lifetime and Uncertainty. *Geophys. Res. Lett.* **2013**, *40*, 4772−4776.

(11) Ghosh, B.; Papanastasiou, D. K.; Burkholder, J. B. Oxalyl chloride, ClC(O)C(O)Cl: UV/vis Spectrum and Cl Atom Photolysis Quantum Yields at 193, 248, and 351 nm. *J. Chem. Phys.* **2012**, *137*, 164315.

(12) Goldfarb, L.; Schmoltner, A.-M.; Gilles, M. K.; Burkholder, J. B.; Ravishankara, A. R. Photodissociation of $ClONO_2$: 1. Atomic Resonance Fluorescence Measurements of Product Quantum Yields. *J. Phys. Chem. A* **1997**, *101*, 6658−6666.

(13) Baklanov, A. V.; Krasnoperov, L. N. Oxalyl Chloride - A Clean Source of Chlorine Atoms for Kinetic Studies. *J. Phys. Chem. A* **2001**, *105*, 97−103.

(14) Papanastasiou, D. K.; Feierabend, K. J.; Burkholder, J. B. Cl_2O Photochemistry: Ultraviolet/vis Absorption Spectrum Temperature Dependence and $O(^3P)$ Quantum Yield at 193 and 248 nm. *J. Chem. Phys.* **2011**, *134*, 204310.

(15) Bravo, I.; Aranda, A.; Hurley, M. D.; Marston, G.; Nutt, D. R.; Shine, K. P.; Smith, K.; Wallington, T. J. Infrared Absorption Spectra, Radiative Efficiencies, and Global Warming Potentials of Perfluorocarbons: Comparison Between Experiment and Theory. *J. Geophys. Res.* **2010**, *115*, D24317.

(16) Baasandorj, M.; Feierabend, K. J.; Burkholder, J. B. Rate Coefficients and ClO Radical Yields in the Reaction of $O(^1D)$ with $CClF_2CCl_2F$, CCl_3CF_3, $CClF_2CClF_2$, and CCl_2FCF_3. *Int. J. Chem. Kinet.* **2011**, *43*, 1−9.

(17) Baasandorj, M.; Fleming, E. L.; Jackman, C. H.; Burkholder, J. B. $O(^1D)$ Kinetic Study of Key Ozone Depleting Substances and Greenhouse Gases. *J. Phys. Chem. A* **2013**, *117*, 2434−2445.

(18) Baasandorj, M.; Hall, B. D.; Burkholder, J. B. Rate Coefficients for the Reaction of $O(^1D)$ with the Atmospherically Long-lived Greenhouse Gases NF_3, SF_5CF_3, CHF_3, C_2F_6, c-C_4F_8, n-C_5F_{12}, and n-C_6F_{14}. *Atmos. Chem. Phys.* **2012**, *12*, 11753−11764.

(19) Sander, S. P.; Abbatt, J.; Barker, J. R.; Burkholder, J. B.; Friedl, R. R.; Golden, D. M.; Huie, R. E.; Kolb, C. E.; Kurylo, M. J.; Moortgat, G. K.; Orkin, V. L.; Wine, P. H. Chemical Kinetics and Photochemical Data for Use in Atmospheric Studies, Evaluation Number 17, JPL Publication 10−6, Jet Propulsion Laboratory, California Institute of Technology Pasadena, CA, 2011; http://jpldataeval.jpl.nasa.gov.

(20) Atkinson, R.; Baulch, D. L.; Cox, R. A.; Crowley, J. N.; Hampson, R. F.; Hynes, R. G.; Jenkin, M. E.; Rossi, M. J.; Troe, J.; Wallington, T. J. Evaluated Kinetic and Photochemical Data for Atmospheric Chemistry: Volume IV Gas-phase Reactions of Organic Halogen Species. *Atmos. Chem. Phys.* **2008**, *8*, 4141−4496.

(21) Feierabend, K. J.; Papanastasiou, D. K.; Burkholder, J. B. ClO Radical Yields in the Reaction of $O(^1D)$ with Cl_2, HCl, Chloromethanes and Chlorofluoromethanes. *J. Phys. Chem. A* **2010**, *114*, 12052−12061.

(22) Papadimitriou, V. C.; Portmann, R. W.; Fahey, D. W.; Mühle, J.; Weiss, R. F.; Burkholder, J. B. Experimental and Theoretical Study of the Atmospheric Chemistry and Global Warming Potential of SO_2F_2. *J. Phys. Chem. A* **2008**, *112*, 12657−12666.

(23) Becke, A. D. Density-functional Thermochemistry. III. The Role of Exact Exchange. *J. Chem. Phys.* **1993**, *98*, 5648−5652.

(24) Perdew, J. P.; Burke, K.; Wang, Y. Generalized Gradient Approximation for the Exchange-correlation Hole of a Many-electron System. *Phys. Rev. B* **1996**, *54*, 16533−16539.

(25) Lazarou, Y. G.; Prosmitis, A. V.; Papadimitriou, V. C.; Papagiannakopoulos, P. Theoretical Calculation of Bond Dissociation Energies and Enthalpies of Formation for Halogenated Molecules. *J. Phys. Chem. A* **2001**, *105*, 6729−6742.

(26) Frisch, M. J.; et al., *Gaussian 03*, revision B.02; Gaussian, Inc.: Pittsburgh, PA, 2003.

(27) Saladino, A. C.; Tang, P. Optimization of Structures and LJ Parameters of 1-chloro-1,2,2-trifluorocyclobutane and 1,2-dichlorohexafluorocyclobutane. *J. Phys. Chem. A* **2004**, *108*, 10560−10564.

(28) Wallington, T. J.; Hurley, M. D. Atmospheric Chemistry of Hexafluorocyclobutene, Octafluorocyclopentene, and Hexafluoro-1,3-butadiene. *Chem. Phys. Lett.* **2011**, *507*, 19−23.

(29) Keller-Rudek, H.; Moortgat, G. K. *MPI-Mainz-UV-VIS Spectral Atlas of Gaseous Molecules*; http://www.uv-vis-spectral-atlas-mainz.org.

(30) Wuebbles, D. J. Chlorocarbon emission scenarios: potential impact on stratospheric ozone. *Geophys. Res. Lett.* **1983**, *88*, 1433−1443.

(31) Fisher, D. A.; Hales, C. H.; Filkin, D. L.; Ko, M. K. W.; Sze, N. D.; Connell, P. S.; Wuebbles, D. J.; Isaksen, I. S. A.; Stordal, F. Model Calculations of the Relative Effects of CFCs and Their Replacements on Stratospheric Ozone. *Nature* **1990**, *344*, 508−512.

(32) Pinnock, S.; Hurley, M. D.; Shine, K. P.; Wallington, T. J.; Smyth, T. J. Radiative Forcing of Climate by Hydrochlorofluorocarbons and Hydrofluorocarbons. *J. Geophys. Res.* **1995**, *100*, 23227−23238.